Journal Pre-proofs

Mathematical modelling of nanoparticle-mediated topical drug delivery to skin tissue

Kevin McLean, Wenbo Zhan

PII: S0378-5173(21)01128-5
DOI: https://doi.org/10.1016/j.ijpharm.2021.121322
Reference: IJP 121322

To appear in: *International Journal of Pharmaceutics*

Received Date: 30 August 2021
Revised Date: 14 November 2021
Accepted Date: 24 November 2021

Please cite this article as: K. McLean, W. Zhan, Mathematical modelling of nanoparticle-mediated topical drug delivery to skin tissue, *International Journal of Pharmaceutics* (2021), doi: https://doi.org/10.1016/j.ijpharm.2021.121322

Mathematical modelling of nanoparticle-mediated topical drug delivery to skin tissue

Kevin McLean, Wenbo Zhan

School of Engineering, King's College, University of Aberdeen, Aberdeen, AB24 3UE, United Kingdom

Correspondence: Dr Wenbo Zhan, School of Engineering, King's College, University of Aberdeen, Aberdeen AB24 3UE, UK, Tel: +44 (0)1224 272511, E-mail: w.zhan@abdn.ac.uk

Submitted for publication in

International Journal of Pharmaceutics

November 2021

Abstract

Nanoparticles have been extensively studied to improve drug delivery outcomes, however, their use in topical delivery remains controversial. Although the feasibility to cross the human skin barrier has been demonstrated in experiments, the risk of low drug concentration in deep tissue still limits the application. In this study, multiphysics modelling is employed to examine the performance of nanoparticle-mediated topical delivery for sending drugs into the deep skin tissue. The pharmacokinetic effect is evaluated based on the drug exposure over time. As compared to the delivery using plain drugs, nanoparticle-mediated topical delivery has the potential to significantly improve the drug exposure in deep skin tissue. Modelling predictions denote that the importance of sufficient long-term drug-skin contact in achieving effective drug deposition in the deep skin tissue. The delivery outcomes are highly sensitive to the release rate. Accelerating the release from nanoparticles in stratum corneum is able to improve the drug exposure in stratum corneum and viable epidermis while resulting in the reductions in dermis and blood. The release rate in stratum corneum and viable epidermis should be well-designed below a threshold for generating effective drug accumulation in dermis and blood. A more localised drug accumulation can be achieved in the capillary-rich region of dermis by increasing the local release rate. The release rate in dermis needs to be optimised to increase the drug exposure in the dermis region where there are fewer blood and lymphatics capillaries. Results from this study can be used to improve the regimen of topical delivery for localised treatment.

Keywords: Drug transport, Localised delivery, Mathematical model, Nanoparticle, Topical delivery

Abbreviations

BD	drug bound with proteins
BL	blood
DM	dermis
FD	free drug
IFP	interstitial fluid pressure
IFV	interstitial fluid velocity
lDM	lower layer of dermis
NP	nanoparticle-encapsulated drug
RD	residue drug
SC	stratum corneum
uDM	upper layer of dermis
VE	viable epidermis

1. Introduction

Topical delivery as a routine drug administration mode has been widely applied in a range of clinical practice, including treatments against dermatological diseases [1], muscle injuries [2] and drug transdermal delivery to the circulatory system [3], etc. Drug formulations in the vehicles are initially applied on the intact skin surface and then penetrate through the skin layers of stratum corneum (SC), viable epidermis (VE) and dermis (DM) in order [4]. Although this administration mode is favourable because of its painless and non-invasive nature, its treatment effectiveness remains to be improved, particularly for sending drugs into the deep skin tissue and subcutis. The disappointing delivery outcome can largely be attributed to the skin barrier of the densely packed SC microstructure [5], resulting in most of the drugs depositing in top skin layers.

Nanoparticles are promising drug carriers with the ability to improve delivery outcomes [6, 7]. With drugs initially encapsulated inside, they can not only reduce drug elimination owing to bioreactions but also release the payloads in a pre-designed, controlled manner after reaching the lesions. Although the potential in topical application, the delivery of hydrophilic substances in particular, has been identified in *ex vivo* experiments [8, 9], nanoparticles are usually believed to be less effective to penetrate SC. However, further studies demonstrate this skin penetration highly depends on the nanoparticle formulation, size and vehicle [10, 11]. Even 200 nm particles are able to pass through rat [12] and pig [13] skin. Human skin is permeable for 6 nm particles from aqueous buffer [14, 15]. However, the penetration of 15 nm particles is only readily from toluene [16]. Moreover, using a lipid-based permeation assay that has a similar lipid composition as the human SC, 100 nm lipid nanoparticles [17] have been found to be able to cross the skin barrier [18]. Despite these, the concentrations of nanoparticles and released drugs in DM could still be significantly low. This study is aimed to evaluate the performance of nanoparticle-mediated topical delivery and identify the possible approaches to improve the

delivery outcomes.

Mathematical modelling including pharmacokinetic modelling and molecular dynamics plays an increasingly important role in studying drug delivery [19-22]. On the one hand, it allows the effects of each influential factor to be examined individually or integrally in the entire delivery process; on the other hand, a parametric study can be performed cost-effectively to identify the opportunities for optimisation [19]. Models have been developed on different scales to study the processes involved in topical delivery. Treating each skin layer as a tissue compartment, the kinetic models are established to describe the drug exchange between skin layers and other related tissues in the body, such as muscles and blood [23, 24]. These models are able to predict the time courses of drug concentration in each compartment, however, the spatial distribution of drugs cannot be obtained. To fill this gap, transport-based models are set up on both the macroscale and microscale to include the geometrical properties of the skin layers. In the macroscale models, each skin layer is considered as a single medium. Hence, the drug delivery processes in and between every medium are governed by the convection-diffusion-reaction equations [25, 26]. Although the drug concentrations in multiple layers can be predicted as a function of time and location, it is important to point out that the microstructures of the skin layers cannot be fully reflected in these models. As a consequence, several different drug processes on the microscale (e.g. transcellular and intercellular transport in SC [27]) are simplified and lumped as one macroscale process (e.g. diffusive transport), resulting in the loss of certain resolutions in the modelling predictions. To overcome this limitation, the microscale models are developed to incorporate the micro-architecture of skin layer explicitly in the geometry [28-30]. The predictions can provide in-depth details and insight into drug interactions with different compositions in the layer. However, these models are usually focused on a limited region in the skin. Simulating the drug transport in multiple skin layers on the microscale is then less computationally viable.

In this study, a macroscale model is applied to simulate the topical delivery of nanoparticle-encapsulated drugs in the multiple skin layers. The model incorporates the key physiological and physicochemical processes involved, including the interstitial fluid flow due to the fluid exchange with the microcirculation, nanoparticle and free drug transport by convection and diffusion through skin layers, drug release dynamics, drug binding with proteins and sorption in the tissue microstructure, blood and lymphatics drainage, and drug elimination due to metabolic reactions. The delivery outcome is evaluated in terms of drug exposure over time using the predicted time course of drug concentration in each skin layer.

2. Materials and Methods

2.1. Mathematical model

The macroscale model consists of two submodules for the transport of interstitial fluid and transport of nanoparticles and released free drugs, respectively. The governing equations together with the model assumptions are given below.

2.1.1. Interstitial fluid transport

SC as a lipid-protein biphasic structure [31] is made up of layers of corneocytes that are sealed by densely packed lipids [32]. Therefore, SC is assumed to be impermeable to the interstitial fluid flow. The transport of incompressible Newtonian interstitial fluid in VE and DM is governed by the mass continuity equation, as

$$\nabla \cdot \mathbf{v} = \begin{cases} F_{\mathrm{bl}} - F_{\mathrm{ly}}, & \text{in uDM} \\ 0, & \text{in VE and lDM} \end{cases} \tag{1}$$

where $\mathbf{v}$ is the interstitial fluid velocity (IFV). F_{bl} is the fluid gain from blood capillaries, and F_{ly} stands for the fluid loss to lymphatics.

Two horizontal plexuses are in the skin. The upper horizontal plexus is situated 1~1.5 mm below the skin surface, while the lower horizontal plexus is at the dermal-subcutaneous interface. Capillaries are extended from the lower horizontal plexus which are bigger vessels [33]. Since the mass transfer and exchange between blood and tissue are mainly through the

capillaries, the lower horizontal plexus is not considered in this study. Given blood capillaries and lymphatic vessels mainly concentrate in the region of DM which is next to the VE-DM interface [22, 34-36], DM is further divided into the upper layer (uDM) and lower layer (lDM), respectively. Those two terms standing for the fluid exchange with the microcirculation are considered locally in uDM, and Starling's law can be applied [37],

$$F_{\mathrm{bl}} = L_{\mathrm{bl}}\frac{S_{\mathrm{bl}}}{V}[p_{\mathrm{bl}} - p_{\mathrm{ir}} - \sigma_T(\pi_{\mathrm{bl}} - \pi_{\mathrm{ir}})] \quad (2)$$

$$F_{\mathrm{ly}} = L_{\mathrm{ly}}\frac{S_{\mathrm{ly}}}{V}[p_{\mathrm{ir}} - p_{\mathrm{ly}}] \quad (3)$$

where L is the hydraulic conductivity of vessel wall, S/V is the surface area of vessel wall per tissue volume, and p refers to the pressure. σ_{T} is the averaged osmotic reflection coefficient for proteins in blood, and π is the osmotic pressure. The subscripts of bl, ly and ir stand for blood, lymphatics and interstitium, respectively. p_{ir} is the interstitial fluid pressure (IFP).

The skin layers of VE and DM are treated as porous media, and Darcy's law is applied under the condition of steady laminar flow, as

$$\mathbf{v} = -\frac{\kappa}{\mu}\nabla p_{\mathrm{ir}} \quad (4)$$

in which μ is the viscosity of interstitial fluid. k refers to Darcy's permeability.

2.1.2. Drug transport

The transport of nanoparticle-encapsulated drugs (NP) and released free drugs (FD) in skin layers of SC, VE and DM are schematically illustrated in **Figure 1**. Nanoparticles are assumed to be stable before entering the skin.

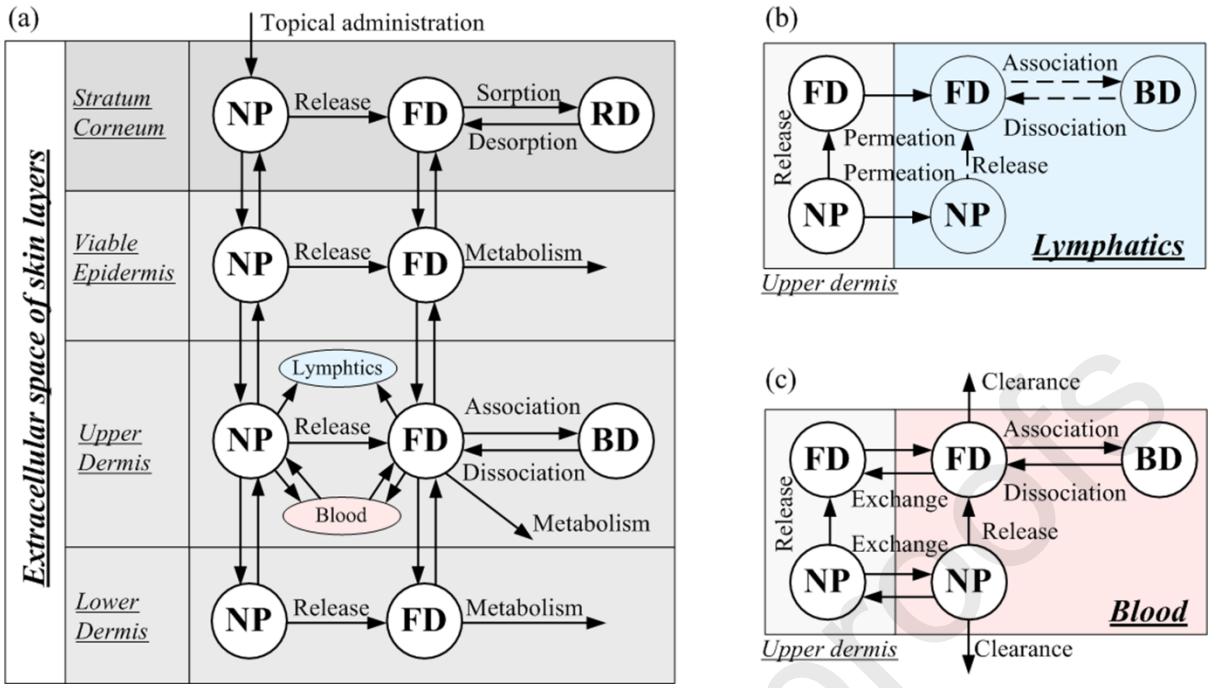

Figure 1. Drug transport in nanoparticle-mediated topical delivery. The overview of transport processes through the skin layers is shown in (a), with a closer look of the drug exchange between skin tissue and lymphatics and blood in (b) and (c), respectively. The function of lymphatics is treated as a sink term for both nanoparticles and free drugs. Therefore, the processes of drug release and binding with proteins in lymphatics are not specified in the model, marked by the dash lines. Given the proteins involved in the binding process, such as albumin, are mainly from the circulatory systems, the drug association and dissociation with proteins are modelled in uDM where blood capillaries exist. The reactions with other proteins are included in the model in terms of metabolic reactions in an integrated manner. This diagram is to show the transport processes of NP and FD only, not referring to the realistic dimension of each skin layer.

Drug transport in SC

The concentration of nanoparticle-encapsulated drugs in SC ($C_{\mathrm{NP,SC}}$) depends on the transport by diffusion and release, as

$$\frac{\partial C_{\mathrm{NP,SC}}}{\partial t} = D_{\mathrm{NP,SC}}\nabla^2 C_{\mathrm{NP,SC}} - k_{\mathrm{rel,SC}} C_{\mathrm{NP,SC}} \tag{5}$$

where $D_{\mathrm{NP,SC}}$ and $k_{\mathrm{rel,SC}}$ are nanoparticle diffusivity and drug release rate in SC, respectively. The released free drugs would bind with tissue compositions and deposit in corneocytes when passing through SC. The concentration ($C_{\mathrm{FD,SC}}$) can be described by

$$\frac{\partial C_{\mathrm{FD,SC}}}{\partial t} = D_{\mathrm{FD,SC}}\nabla^2 C_{\mathrm{FD,SC}} + k_{\mathrm{rel,SC}} C_{\mathrm{NP,SC}} - k_{\mathrm{SP}} C_{\mathrm{FD,SC}} + k_{\mathrm{DP}} C_{\mathrm{RD,SC}} \tag{6}$$

where $D_{\mathrm{FD,SC}}$ is the diffusivity of free drugs. k_{SP} and k_{DP} are the constant rate of sorption and

desorption in SC, respectively. The concentration of residue drugs (RD) in SC ($C_{\mathrm{RD,SC}}$) [38] is governed by

$$\frac{dC_{\mathrm{RD,SC}}}{dt} = k_{\mathrm{SP}}C_{\mathrm{DF,SC}} - k_{\mathrm{DP}}C_{\mathrm{RD,SC}} \quad (7)$$

Drug transport in VE

The nanoparticle-encapsulated drugs transport in VE by diffusion driven by the concentration gradient and drug release. Since the interstitial fluid velocity is significantly low, the drug transport by convection is neglected in VE. The concentration ($C_{\mathrm{NP,VE}}$) can be interpreted by

$$\frac{\partial C_{\mathrm{NP,VE}}}{\partial t} = D_{\mathrm{NP,VE}}\nabla^2 C_{\mathrm{NP,VE}} - k_{\mathrm{rel,VE}}C_{\mathrm{NP,VE}} \quad (8)$$

where $D_{\mathrm{NP,VE}}$ and $k_{\mathrm{rel,VE}}$ are the local nanoparticle diffusivity and release rate, respectively. To be different from the transport in SC, the free drugs in VE would be eliminated due to metabolic reactions. The concentration ($C_{\mathrm{FD,VE}}$) can be calculated by

$$\frac{\partial C_{\mathrm{FD,VE}}}{\partial t} = D_{\mathrm{FD,VE}}\nabla^2 C_{\mathrm{FD,VE}} + k_{\mathrm{rel,VE}}C_{\mathrm{FD,VE}} - \frac{V_{\max}C_{\mathrm{FD,VE}}}{v_{\mathrm{m}} + C_{\mathrm{FD,VE}}} \quad (9)$$

in which $D_{\mathrm{FD,VE}}$ is the diffusivity of free drugs in VE. $V_{\max}$ and v_{m} are the reaction constant rates of metabolic reactions.

Drug transport in DM

The transport of nanoparticle-encapsulated drugs in DM is determined by diffusion and convection, drug release, and drug exchange between the DM interstitial space, blood and lymphatics. This can be expressed as [39, 40]

$$\frac{\partial C_{\mathrm{NP,DM}}}{\partial t} = D_{\mathrm{NP,DM}}\nabla^2 C_{\mathrm{NP,DM}} - \nabla\cdot(\mathbf{v}C_{\mathrm{NP,DM}}) - k_{\mathrm{rel,DM}}C_{\mathrm{NP,DM}} - Ex(C_{\mathrm{NP,BL}},C_{\mathrm{NP,DM}}) - F_{\mathrm{ly}}C_{\mathrm{NP,DM}} \quad (10)$$

in which $C_{\mathrm{NP,DM}}$ is the concentration of nanoparticle-encapsulated drugs in DM. $D_{\mathrm{NP,DM}}$ refers to the nanoparticle diffusivity in DM, and $k_{\mathrm{rel,DM}}$ is the local drug release rate. The exchange of nanoparticle-encapsulated drugs between the blood (BL) and DM is presented by $Ex(C_{\mathrm{NP,BL}},C_{\mathrm{NP,DM}})$ that is defined as

$$Ex(C_{\mathrm{NP,BL}},C_{\mathrm{NP,DM}}) = P_{\mathrm{NP}}\frac{S_{\mathrm{bl}}}{V}(C_{\mathrm{NP,DM}} - C_{\mathrm{NP,BL}})\frac{\mathrm{Pe}_{\mathrm{tb,NP}}}{e^{\mathrm{Pe}_{\mathrm{tb,NP}}}-1} - F_{\mathrm{bl}}(1-\sigma_{\mathrm{NP}})C_{\mathrm{NP,BL}} \quad (11)$$

in which $C_{\mathrm{NP,BL}}$ is the concentration in blood. σ_{NP} is the osmotic reflection coefficient for nanoparticles. P_{NP} stands for the nanoparticle transvascular permeability. The transvascular Péclet number of nanoparticles is $\mathrm{Pe}_{\mathrm{tb,NP}} = \frac{F_{\mathrm{bl}}(1-\sigma_{\mathrm{NP}})}{P_{\mathrm{NP}}\,S_{\mathrm{bl}}/V}$.

Similarly, the concentration of free drugs in DM ($C_{\mathrm{FD,DM}}$) is governed by convection and diffusion, drug release from nanoparticles, elimination due to metabolic reactions, binding with proteins and exchange between the DM interstitial space, blood and lymphatics, as

$$\frac{\partial C_{\mathrm{FD,DM}}}{\partial t} = D_{\mathrm{FD,DM}}\nabla^2 C_{\mathrm{FD,DM}} - \nabla\cdot(\mathbf{v}C_{\mathrm{FD,DM}}) + k_{\mathrm{rel,DM}}C_{\mathrm{FD,DM}} - \frac{V_{\max}C_{\mathrm{FD,DM}}}{v_{\mathrm{m}}+C_{\mathrm{FD,DM}}} - k_{\mathrm{AR}}C_{\mathrm{FD,DM}} + k_{\mathrm{DR}}$$
$$C_{\mathrm{BD,DM}} - Ex(C_{\mathrm{FD,BL}},C_{\mathrm{FD,DM}}) - F_{\mathrm{ly}}C_{\mathrm{FD,DM}} \quad (12)$$

where $D_{\mathrm{FD,DM}}$ is the diffusivity of free drugs in DM. k_{AR} and k_{DR} are the reaction constant rates of association and disassociation with proteins, respectively. The exchange of free drugs between DM and BL, $Ex(C_{\mathrm{FD,BL}},C_{\mathrm{FD,DM}})$, has the same definition in **Eq.(11)** using the concentrations and properties of free drugs. The concentration of bound drugs in DM ($C_{\mathrm{BD,DM}}$) is governed by

$$\frac{dC_{\mathrm{BD,DM}}}{dt} = k_{\mathrm{AR}}C_{\mathrm{FD,DM}} - k_{\mathrm{DR}}C_{\mathrm{BD,DM}} \quad (13)$$

Drug transport in BL

The intravascular concentration of nanoparticle-encapsulated drugs ($C_{\mathrm{NP,BL}}$) depends on the transport from uDM, drug release from nanoparticles in blood and drug plasma clearance, as

$$\frac{dC_{\mathrm{NP,BL}}}{dt} = \frac{V_{\mathrm{uDM}}}{V_{\mathrm{dis,NP}}}Ex(C_{\mathrm{NP,BL}},C_{\mathrm{NP,DM}}) - k_{\mathrm{rel,BL}}C_{\mathrm{NP,BL}} - k_{\mathrm{clr,NP}}C_{\mathrm{NP,BL}} \quad (14)$$

in which V_{uDM} and $V_{\mathrm{dis,NP}}$ are the volume of uDM and distribution volume of nanoparticles, respectively. $k_{\mathrm{rel,BL}}$ is the drug release rate in blood. $k_{\mathrm{clr,NP}}$ is the plasma clearance of nanoparticles.

The transport of free drugs in blood is governed by the exchange with uDM, local drug release,

plasma clearance and binding with proteins, defined as

$$\frac{dC_{\mathrm{FD,BL}}}{dt} = \frac{V_{\mathrm{uDM}}}{V_{\mathrm{dis,FD}}} Ex(C_{\mathrm{FD,BL}}, C_{\mathrm{FD,DM}}) + k_{\mathrm{rel,BL}} C_{\mathrm{NP,BL}} - k_{\mathrm{clr,FD}} C_{\mathrm{FD,BL}} - k_{\mathrm{AR}} C_{\mathrm{FD,BL}} + k_{\mathrm{DR}} C_{\mathrm{BD,BL}}$$

(15)

where $V_{\mathrm{dis,FD}}$ is the distribution volume of free drugs, $k_{\mathrm{clr,FD}}$ stands for the plasma clearance of free drugs. The drug-binding in BL ($C_{\mathrm{BD,BL}}$) is governed by

$$\frac{dC_{\mathrm{BD,BL}}}{dt} = k_{\mathrm{AR}} C_{\mathrm{FD,BL}} - k_{\mathrm{DR}} C_{\mathrm{BD,BL}} \quad (16)$$

2.2. Model geometry

The mathematical modelling of nanoparticle-mediated topical delivery is conducted in a 1D configuration as shown in **Figure 2**. The dimensions of skin layers including SC, VE, uDM and lDM are given in **Table 1**. The final computational mesh consists of 1,597 structured elements after performing the mesh-independence test.

Figure 2. Model geometry. The information of layer dimension is listed in Table 1.

2.3. Model parameters

Given the time window of this modelling study is much shorter as compared to the growth rate and remodelling rate of the skin and circulatory systems, the properties of drugs and tissues are assumed to be constant. The baseline values of model parameters are summarised in **Table 1** and **Table 2** for skin tissues and drugs, respectively. Doxorubicin is used in this study as a representative drug since it has been applied to treat melanoma [41-43], which could local in the skin with different depths depending on the cancer stage [44, 45]. The justification for the choices of key parameters is given below.

Thickness of skin layers (d)

The thickness of each skin layer could vary considerably depending on multiple factors, such as location and age. On average [22], SC was measured 10~30 μm on face, forearm and

abdomen, while its thickness could increase to 50 μm if diseased. The thickness of VE is located in the range of 31~637 μm [46], with the minimum and maximum value obtained at penis and sole, respectively. Therefore, these two layers are specified as 35 μm and 350 μm thick. DM is 1200 μm thick based on the reported range of 469~1492 μm [46]. The thickness of uDM is in the range of 100~200 μm [22], so that the value of 150 μm is used.

Tissue permeability (κ)

Tissue permeability measures the capability of the tissue to allow for the interstitial fluid flow passing through. This parameter of the general non-tumoural tissue was firstly applied in Ref [37], and then specified as 4.52×10^{-18} m^2 in Ref. [40]. Moreover, the value of 6.40×10^{-15} m^2 was also applied [47]. Most of the normal tissues including VE and DM are physiologically different. However, they are mostly aqueous phases. As compared to SC, VE and DM have less contribution to the overall skin resistance [22]. Therefore, the same tissue permeability of 1.0×10^{-16} m^2 is applied to VE and DM.

Partition coefficient (K)

A partition coefficient is the ratio of the drug concentrations in two different media. Based on Ref. [48] where the partition coefficients of forty-four drugs are summarised, a correlation between the drug K_{SC} and $K_{\mathrm{o/w}}$ is established as **Eq.(17)**. The result of curve fitting is shown in **Figure 3**.

$$\log K_{\mathrm{SC}} = 0.58297 \log K_{\mathrm{o/w}} + 0.00512 \tag{17}$$

Given the $K_{\mathrm{o/w}}$ of doxorubicin was measured as 0.0557 [49] and 0.0479 [50], its K_{SC} is estimated as 0.19 and 0.17 correspondingly. Hence, 0.18 is used in this study. The equivalent partition coefficient of nanoparticles in octanol/water ($\tilde{K}_{\mathrm{o/w}}$) is strongly dependent on the formulation. As it was measured in the range of 0.036~13.98 [51, 52], the equivalent $\tilde{K}_{\mathrm{SC}}$ of nanoparticles is estimated as 0.14~4.71 using **Eq.(17)**. Therefore, the average value of 2.75 is applied. K_{VE} of both nanoparticles and free drugs are assumed to be 1.0 since VE and DM are

aqueous membranes [22].

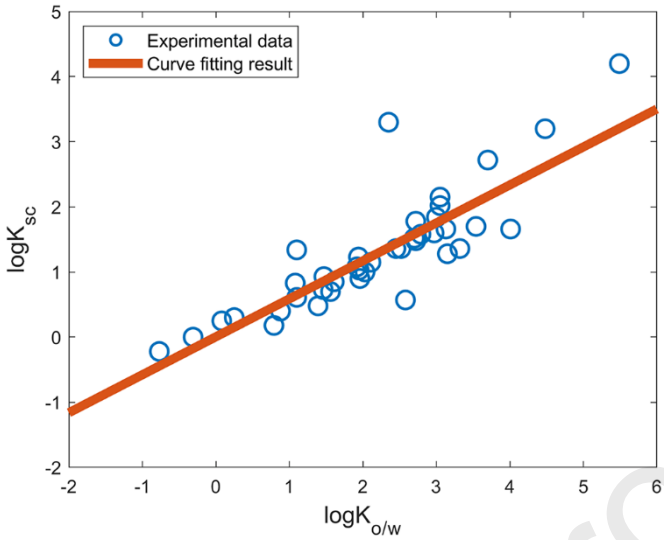

Figure 3. The relationship between drug K_{SC} and $K_{o/w}$. The coefficient of determination (R^2) is 0.71. Experimental data is extracted from Ref. [48].

Drug diffusivity (D)

Diffusivity describes the capability of drug transport driven by the concentration gradient in tissue. Since this parameter spans in the range from 2.0×10^{-11} to 2.0×10^{-10} m^2/s for small molecule drugs in normal tissues [53], 1.0×10^{-10} m^2/s is used for the free drugs in VE and DM. The diffusivity of nanoparticles is determined by serval factors, including the particle size and surface charge, etc. The value for a 100 nm doxorubicin-encapsulated nanoparticle was measured as $7.65 \times 10^{-11} m^2/s$ [54] in collagen, which is one the major compositions of tissue extracellular matrix where drugs transport in. By fitting to the measured concentration profiles, the diffusivity of 100 nm and 10 nm particles were calculated as $2.2 \times 10^{-12} m^2/s$ and $2.3 \times 10^{-11} m^2/s$, respectively, in collagen matrix [55]. The diffusivity of 100 nm liposomes in tissue was reported as $2.4 \times 10^{-13} m^2/s$, and the value was used in the modelling study [56]. Given both the 6 nm [14, 15] and 100 nm [17, 18] particles showed the potential to permeate human skin, the lower bound value of 1.0×10^{-13} m^2/s is applied as the nanoparticle diffusivity in VE and DM.

Given the diffusivity of small molecules in SC is at least 3 orders lower than in VE [57], the

free drug diffusivity in SC is set as 1.0×10^{-14} m^2/s. On the other hand, although the phenomenon of nanoparticles diffusing through SC was observed, there is a lack of studies measuring the nanoparticle diffusivity in SC. As an alternative, the same correlation between free drug diffusivity in SC and VE is used. The diffusivity of nanoparticles in SC thereby is estimated as 1.0×10^{-17} m^2/s in this study.

Release rate from nanoparticles (k_{rel})

Release rate stands for the time scale for the nanoparticles to release the payloads. It depends on the nanoparticle formulation and environment such as temperature [58] and pH value [59], etc. For instance, thermosensitive nanoparticles are able to release the drugs in a few seconds when the environmental temperature is above a pre-designed threshold [60]. In contrast, stealth nanoparticles can provide continuous release over weeks [61]. The release rate is commonly located in the range from 1.0×10^{-6} to 1.0×10^{-2} s^{-1}, which will be used in this study to examine the effects of release rate on the outcomes of nanoparticle-mediated topical delivery, with the baseline value set as 1.0×10^{-4} s^{-1}.

Drug-skin contact duration (T)

Drug-skin contact duration is directly related to the dose for administration. Different vehicles have been developed for providing a sustainable drug supply. This duration could vary considerably subject to the vehicle formulation. For instance, the nanoemulsion gel [62] could release the payload in 12 hours. A 48-hour time window can be achieved using a biphasic gel system [63]. A hydrogel was developed with the ability to offer a 24-hour continuous supply of the nanoparticle stabilised liposomes for topical delivery [64]. As the hydrogel was applied once daily in the *in vivo* experiment, the same drug-skin contact duration of 24 hours is used.

Table 1. Transport properties of the different layers of skin tissue

Symbol	Parameter	Unit	SC	VE	DM	Source
d	Thickness of the skin layer	μm	35	350	1200	[22, 46]
κ	Permeability to interstitial fluid	M^2	0	1.0×10^{-16}	1.0×10^{-16}	[65]
μ	Viscosity of interstitial fluid	Pas	7.8×10^{-4}	7.8×10^{-4}	7.8×10^{-4}	[40]
ρ	Density of interstitial fluid	kg/m^3	1000	1000	1000	[66]
π_b	Osmotic pressure of blood	Pa	-	-	2670	[37]
π_i	Osmotic pressure of interstitial fluid	Pa	-	-	1330	[37]
σ_T	Osmotic reflection coefficient for blood proteins	-	-	-	0.91	[37]
L_b	Hydraulic conductivity of the blood vessel wall	m/Pa/s	-	-	2.7×10^{-12}	[37]
p_b	Intracapillary pressure	Pa	-	-	2080	[37]
S_b/V	Capillary surface area per tissue volume	m^{-1}	-	-	100	[67, 68]
$L_l S_l/V$	Transport rate of interstitial fluid to lymphatics	$Pa^{-1}s^{-1}$	-	-	4.2×10^{-7}	[37]
p_l	Intra-lymphatic pressure	Pa	-	-	0	[37]

Table 2. Transport properties of chemotherapeutic agents

Symbol	Parameter	Unit	Nanoparticle	Free drug	Source
D_{SC}	Diffusivity in SC	m^2/s	1.0×10^{-17}	1.0×10^{-14}	[53, 57]
D_{VE}	Diffusivity in VE	m^2/s	1.0×10^{-13}	1.0×10^{-10}	[57]
D_{DM}	Diffusivity in DM	m^2/s	1.0×10^{-13}	1.0×10^{-10}	[57]
K_{SC}	Partition coefficient between delivery vehicle and SC	-	2.75	0.18	[48]
K_{VE}	Partition coefficient between delivery vehicle and VE	-	1.0	1.0	[22]
k_{rel}	Release rate	s^{-1}	1.0×10^{-4}	-	[69]
k_{BR}	Sorption rate in SC	s^{-1}	-	7.5×10^{-4}	[38]
k_{UR}	Desorption rate in SC	s^{-1}	-	7.5×10^{-4}	[38]
V_{max}	Michaelis–Menten parameter for metabolic reaction	$mol/m^3/s$	-	0.152	[70]
v_m	Michaelis–Menten parameter for metabolic reaction	mol/m^3	-	6.7×10^{-3}	[70]
k_{AR}	Association rate of drugs with proteins	s^{-1}	-	0.833	[71]
k_{DR}	Dissociation rate of drugs with proteins	s^{-1}	-	0.278	[71]
P	Transvascular permeability	m/s	0	3.8×10^{-7}	[72, 73]
k_{clr}	Clearance rate in blood	s^{-1}	5.0×10^{-5}	1.0×10^{-4}	[74-76]
V_{dis}	Distribution volume	m^3	1.8×10^{-2}	2.0×10^{-2}	[71, 74]

2.4. Numerical methods

The mathematical model is implemented in a Finite Element Method-based code package COMSOL Multiphysics (COMSOL Inc., Stockholm, Sweden) for generating numerical solutions. A fixed time step of 1.0×10^{-3} s is deemed sufficiently fine based on the time step independence test. The drug transport is assumed to have no impact on IFP and IFV in skin layers. Therefore, governing equations for the transport of interstitial fluid are solved first to

generate a steady-state solution. The obtained IFP and IFV are then imported into the drug transport model for simulating the nanoparticle and free drug transport in the skin layers. The initial concentrations of all drugs are assumed to be zero in the entire domain.

2.5. Boundary conditions

A constant concentration of nanoparticle-encapsulated drugs of 1.0 M is applied on the top of SC layer for administration; while the local flux of free drugs is assumed to be zero. The velocity of interstitial fluid flow is zero at the SC-VE interface since SC is impermeable to the flow. The transport of nanoparticles and free drugs at this interface follow the relationships [25] described in **Eq.(18)**. Given VE and DM have similar transport properties [22], the continuous boundary condition is applied at the VE-DM interface. The constant pressure of 0 Pa is imposed on the bottom boundary of DM, where the concentrations of drugs are set as zero.

$$\begin{aligned} C_{\mathrm{NP,VE}} &= K_{\mathrm{NP,VE}} C_{\mathrm{NP,SC}} / K_{\mathrm{NP,SC}} \quad & -D_{\mathrm{NP,VE}} \frac{\partial C_{\mathrm{NP,VE}}}{\partial x} &= -D_{\mathrm{NP,SC}} \frac{\partial C_{\mathrm{NP,SC}}}{\partial x} \\ C_{\mathrm{FD,VE}} &= K_{\mathrm{FD,VE}} C_{\mathrm{FD,SC}} / K_{\mathrm{FD,SC}} \quad & -D_{\mathrm{FD,VE}} \frac{\partial C_{\mathrm{FD,VE}}}{\partial x} &= -D_{\mathrm{FD,SC}} \frac{\partial C_{\mathrm{FD,SC}}}{\partial x} \end{aligned} \tag{18}$$

2.6. Quantification of delivery outcomes

The delivery outcomes of nanoparticle-mediated topical delivery under different conditions are evaluated using the quantitative indexes defined below.

2.6.1. Spatial averaged concentration

Drug concentration is determined by the transport processes illustrated in **Figure 1**, and varies throughout each skin layer. The parameter of spatial averaged concentration is used to examine the drug accumulation in the entire skin layer, as

$$C = \frac{\Sigma C_i V_i}{\Sigma V_i} = \frac{\Sigma C_i V_i}{V_{\mathrm{layer}}} \tag{19}$$

where V_{layer} is the volume of the layer.

2.6.2. Effective drug exposure over time

This delivery outcome could be evaluated by the drug exposure over time (AUC), which is

defined as the area under the curve of spatial averaged concentration against time, as

$$AUC = \sum_0^T Ct \tag{20}$$

where T is the drug-skin contact duration.

3. Results

3.1. Baseline study

Driven by the transvascular pressure gradient, plasma is able to transport from blood into the interstitial space of uDM and thus promotes the flow of interstitial fluid in VE and lDM. The lost fluid would be drained by lymphatics out of the tissue as a result of the pressure difference across the lymphatic wall. Governing equations are solved in the entire domain to obtain the flow in VE and DM, subject to the model parameters in **Table 1**. Results in **Figure 4** shows that IFP reduces all the way through the skin layers from the SC-VE interface down to the far end of DM. Whereas the IFV exhibits the inverse pattern of distribution, with the higher velocity presenting in the deeper site of the skin. The IFV reaches its lowest level at the SC-VE interface owing to the impermeable nature of SC to the flow. It is also important to note that the IFV remains on the scale of 10^{-11} m/s, demonstrating that the interstitial fluid flow is fairly slow in the entire skin tissue.

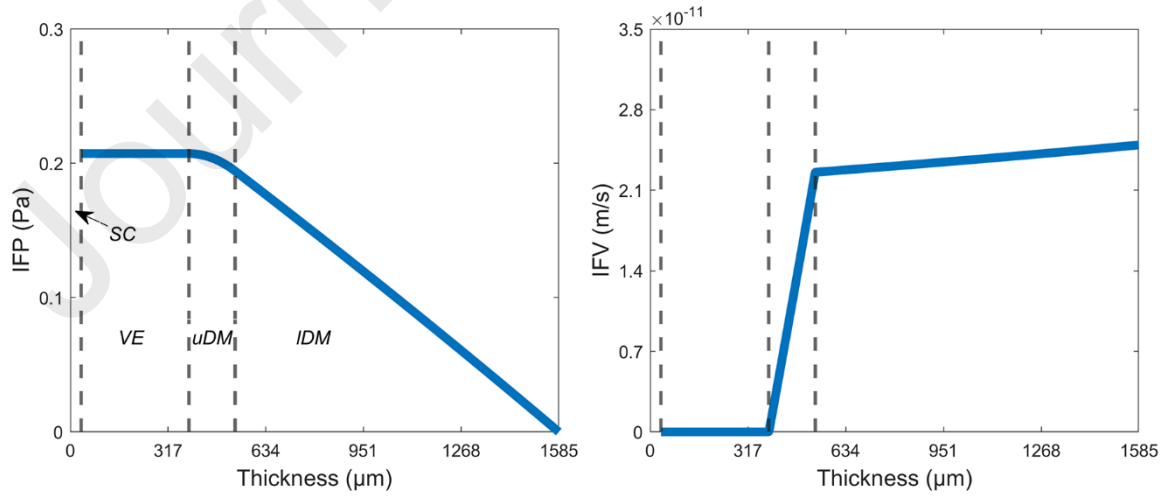

Figure 4. The predicted pressure (left) and velocity (right) of interstitial fluid flow in skin layers.

The time courses of spatial averaged concentration of nanoparticle-encapsulated drugs in skin

layers and blood are presented in **Figure 5**. Since SC is the first skin layer exposed to the drugs, its concentration raises immediately after the administration starts until reaching a plateau. This is owing to the dynamic equilibrium established between the source term of drug administration and the sink terms of drug loss due to drug release and transport into the downstream layers. In contrast, the drug accumulation presents different patterns in the rest skin layers. The concentrations of nanoparticles remain low in about the first 18 hours, followed by dramatic increases until the end of this treatment cycle. This delay is largely due to the significantly high resistance in SC and the low diffusivity of nanoparticles, which effectively slow down the drug transport to the deep sites of skin. Moreover, the intravascular concentration of nanoparticles is zero all the time. This is because of the nanoparticle's large dimension, which prevents this drug delivery system to cross the continuous non-fenestrated capillaries in skin [73]. The significant differences in the time scale of drug accumulation in tissue compartments highlight the importance of performing a sustainable topical delivery over time in order to obtain effective drug accumulation in deep skin layers.

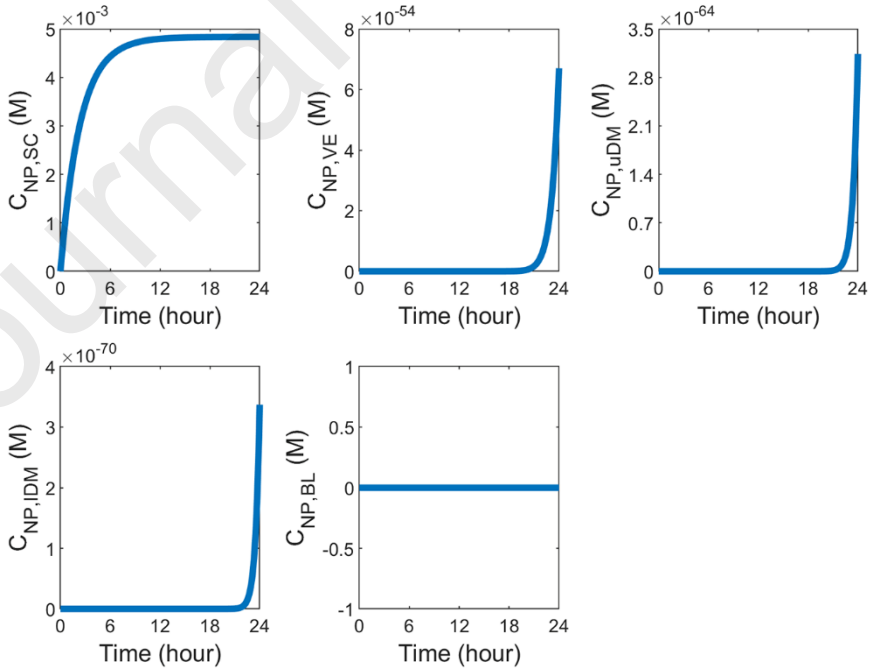

Figure 5. Spatial averaged concentration of nanoparticle-encapsulated drugs as a function of time in skin layers and blood.

The time courses of free drug concentration in each tissue compartment and blood are represented in **Figure 6**. It is not surprising that the concentration in SC increases once the treatment starts. However, to be different from the nanoparticles shown in **Figure 5,** 24 hours are even insufficient for free drugs to reach the dynamic equilibrium in SC. A similar trend can be found in VE with a 6-hour delay. This is followed by the concentrations in DM, where free drugs begin to accumulate about 20 hours after the treatment starts. The concentration in BL presents a similar trend as in uDM, since all the free drugs in the blood are from uDM by the transvascular exchange. Furthermore, the concentrations of free drugs and drugs bound with proteins change simultaneously, indicating the two-way dynamic process of drug binding with proteins takes place on a small time scale. A similar finding can be found for the process of drug sorption in SC, as the curves of concentrations of free drugs and residue drugs are nearly overlapped. In addition, as compared to nanoparticles, the free drug concentration is several orders higher in VE. This would indicate that the accumulation of free drugs in VE is determined by the drug release from nanoparticles in this layer and the transport of free drugs from the upstream layer of SC.

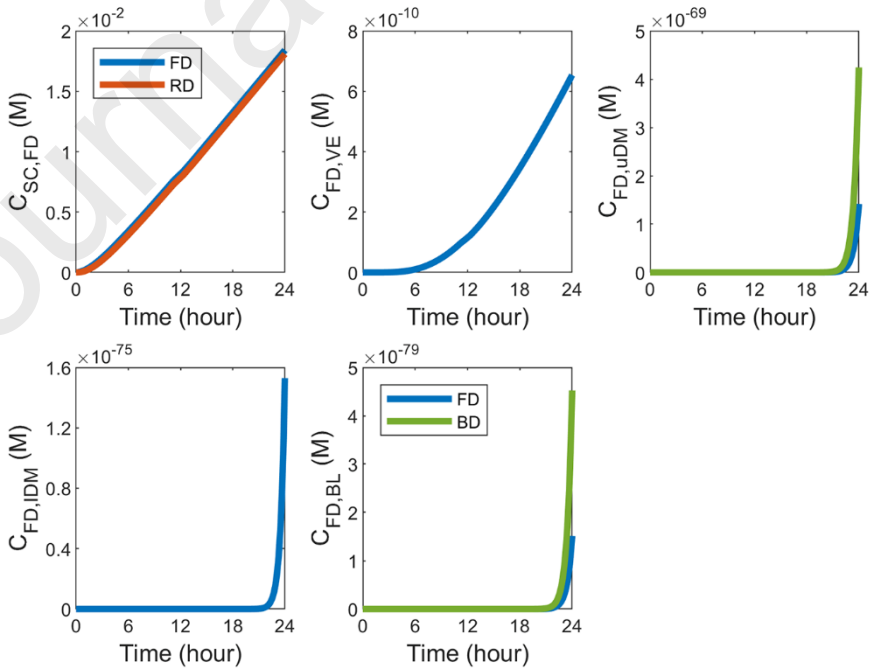

Figure 6. Spatial averaged concentration of released drugs as a function of time in skin layers and blood.

The outcomes of nanoparticle-mediated topical delivery, evaluated by AUC, is compared to that of conventional topical delivery using plain drugs in **Figure 7**. The application of nanoparticles can not only effectively reduce the drug exposure in SC and VE, but also significantly increase the delivery outcomes in DM and BL by several orders. This comparison demonstrates the advantages of nanoparticles in overcoming the skin barrier for sending drugs into deep sites of the skin and the blood circulatory system.

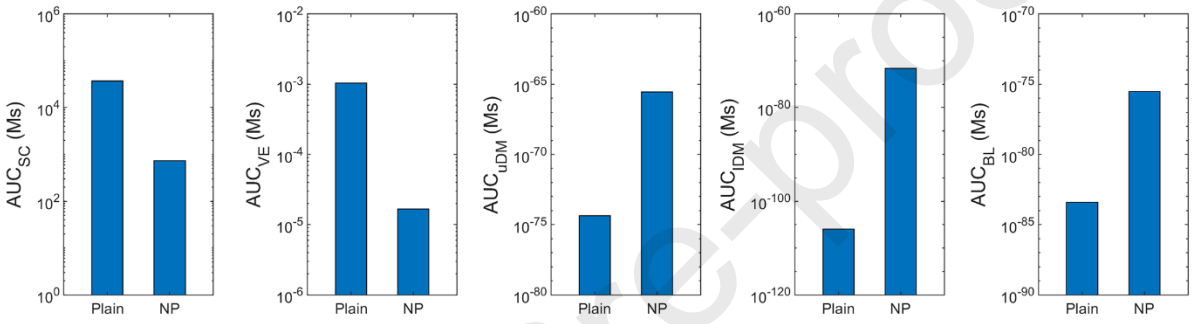

Figure 7. Comparison of drug exposure over time ($AUC_{24\text{hour}}$) in different skin layers and blood using nanoparticles and plain drugs.

3.2. Effect of release rate in SC ($k_{\text{rel,SC}}$)

The impacts of release rate in SC on nanoparticle-encapsulated drug concentrations in different skin layers and blood are shown in **Figure 8**. Results denote that increasing the drug release rate in SC can significantly reduce the concentrations of nanoparticle-encapsulated drugs in all the skin layers. This is because nanoparticles transport through the skin layers of SC, VE, uDM and lDM in order. Fewer nanoparticles are available to transport to the downstream layers when the release in SC is enhanced. Further comparisons show that the release rate $k_{\text{rel,sc}} = 1.0 \times 10^{-2}$ s^{-1} and $k_{\text{rel,sc}} = 1.0 \times 10^{-3}$ s^{-1} could result in comparable drug concentrations, while the concentration can be largely raised by reducing $k_{\text{rel,sc}}$ from 1.0×10^{-3} s^{-1} to 1.0×10^{-5}s^{-1}. This implies a non-linear, inverse correlation between $k_{\text{rel,sc}}$ and the concentration of the nanoparticle-encapsulated drugs in all the skin layers.

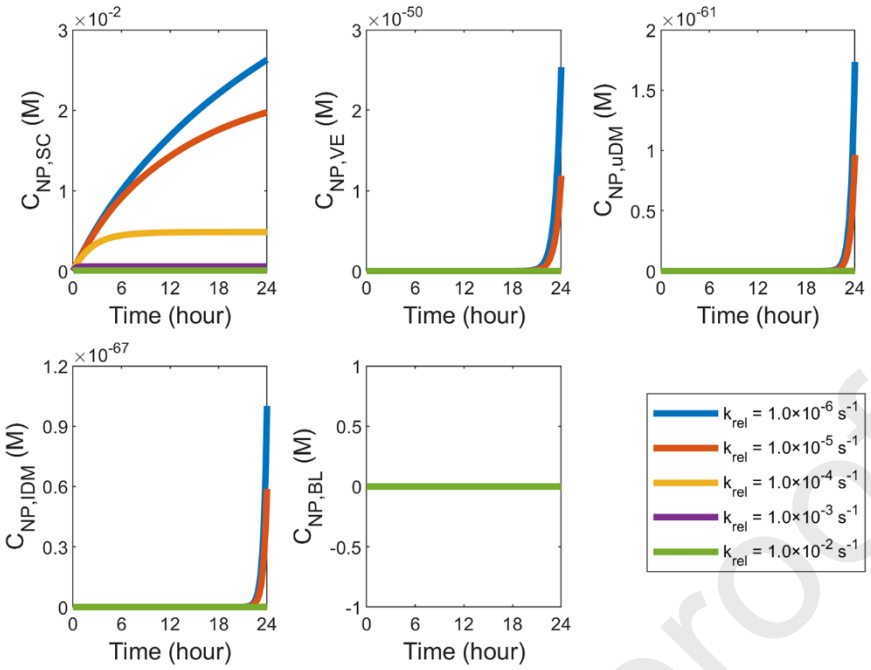

Figure 8. Time courses of nanoparticle-encapsulated drug concentration is skin layers and blood using nanoparticles with different release rates in SC.

Figure 9 compares the free drug concentration in different layers and blood when the release rate in SC changes. A higher concentration can be obtained in SC when the local release rate is increased. A similar trend can also be found in VE, indicating the released drugs in SC could successfully transport into VE. However, the free drug concentration is inversely correlated to $k_{\mathrm{rel,sc}}$ in DM and BL, with the higher concentrations reached for the nanoparticles with slow-release in SC. These trends imply that the free drug concentrations in the deep skin layers are mainly dependent on the local drug release from nanoparticles. This location-dependent impact could be largely due to the metabolic reactions in VE that could effectively eliminate free drugs, reducing the amount of free drugs that could transport from VE to the downstream.

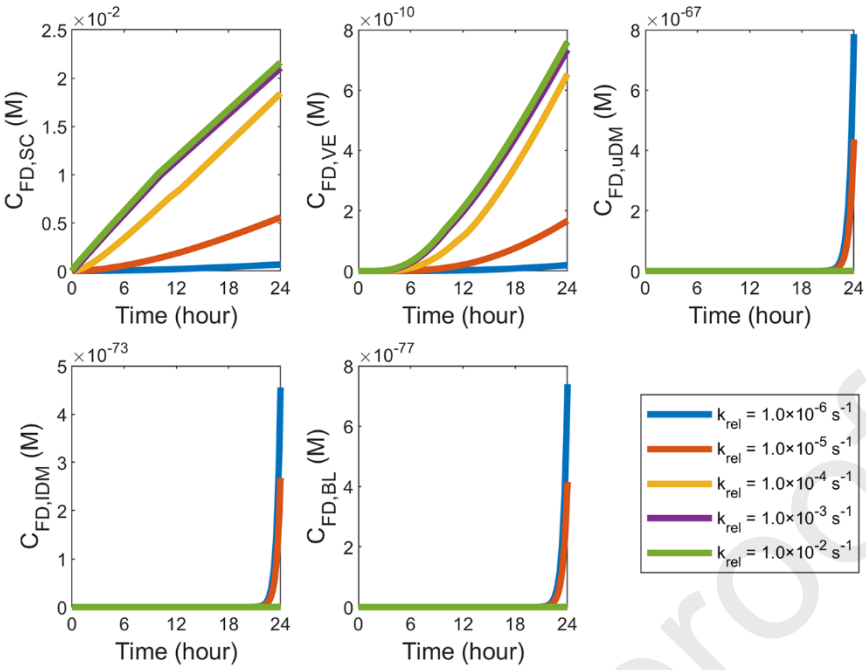

Figure 9. Time courses of free drug concentration is skin layers and blood using nanoparticles with different release rates in SC.

The delivery outcomes of nanoparticles with different SC release rates are compared in **Figure 10**. Using the nanoparticles with fast SC-release would improve the treatment in SC and VE. On the contrary, the drug exposure in DM and BL decreases with the increase of $k_{\mathrm{rel,SC}}$. Consequently, accelerating the drug release in SC is a promising means to achieve localised drug delivery in the top two skin layers, while the risk of side effects in the deep skin tissue and systemic toxicity can also be reduced. More importantly, nanoparticles with the $k_{\mathrm{rel,SC}}$ greater than 1.0×10^{-4} s^{-1} would result in most of the free drugs accumulating in the top two layers, whereas the drug exposure in DM and BL is invisible.

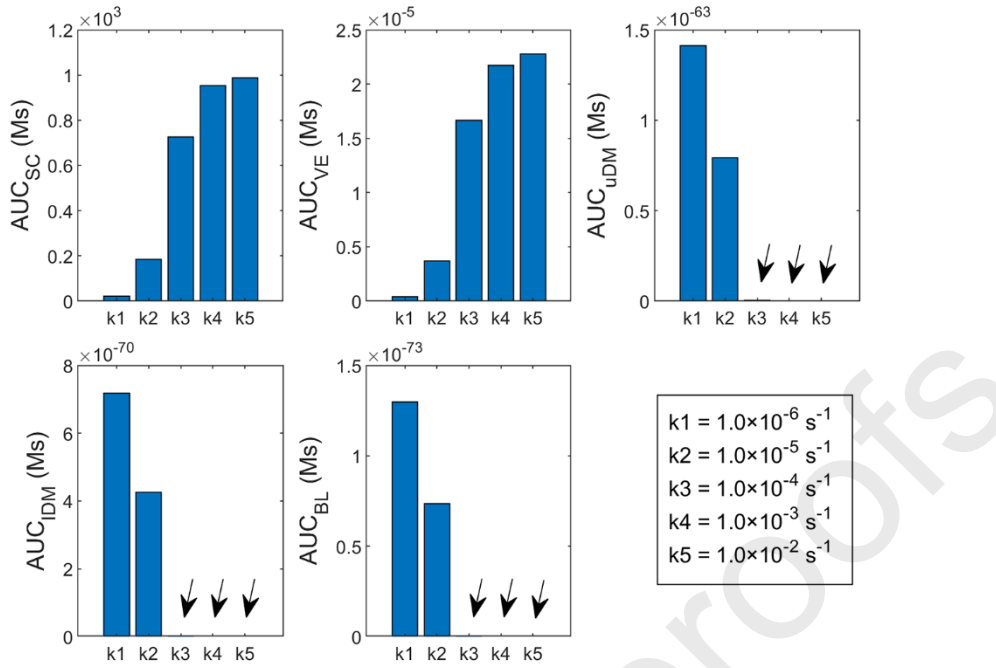

Figure 10. Drug exposure over time ($AUC_{24\text{hour}}$) of skin layers and blood using nanoparticles with different release rates in SC.

3.3. Effect of release rate in VE ($k_{\text{rel,VE}}$)

Figure 11 shows the impacts of release rate in VE on the nanoparticle-encapsulated drug concentration in the skin and blood. Increasing this release rate is effective to reduce the concentration of nanoparticles in VE, as the payload can be quickly released locally. However, the concentration in the upstream layer of SC is insensitive to the changes in $k_{\text{rel,VE}}$. On the other hand, due to the fast release in VE when $k_{\text{rel,VE}}$ is high, there are fewer nanoparticle-encapsulated drugs available to reach the downstream layer of DM. Quantitative comparisons show that the concentrations in DM would be significantly low when $k_{\text{rel,VE}}$ is greater than 1.0×10^{-4} s^{-1}.

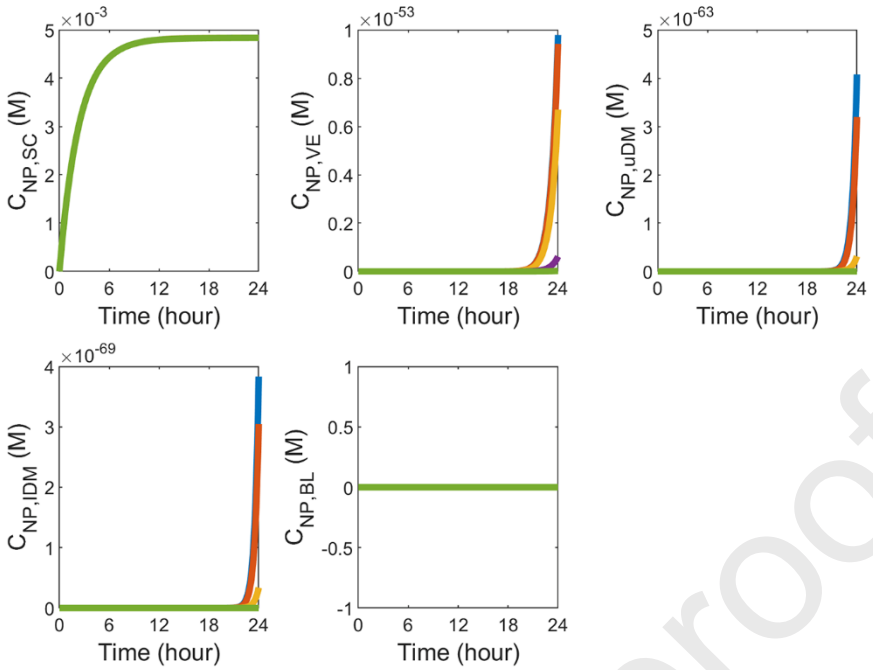

Figure 11. Time courses of nanoparticle-encapsulated drug concentration is skin layers and blood using nanoparticles with different release rates in VE.

The concentrations of free drugs in skin layers and blood in the delivery using nanoparticles with different release rates in VE are shown in **Figure 12**. A negative relationship can be found between $k_{\mathrm{rel,VE}}$ and the free drug concentration in VE. This might be owing to the nanoparticle properties. The nature of hydrophobicity is beneficial to reduce the resistance for the nanoparticles to transport in SC. However, it would also retard the transport from SC to VE that is an aqueous membrane, as indicated by Eq.(18). This consequently limits the amount of nanoparticles entering the VE. Although drugs can quickly be released from the nanoparticles with a high $k_{\mathrm{rel,VE}}$, the released free drugs could also be fast eliminated due to the local metabolic reactions. Hence, the concentration of free drugs would be low when the high $k_{\mathrm{rel,VE}}$ nanoparticles are used. Moreover, an interesting finding is in SC, where the free drug concentration presents a similar trend as in VE. This backward influence can be attributed to the enlarged concentration gradient across the SC-VE interface. It could drive more free drugs to transport from SC to VE, and thereby lead to the decrease of the free drug accumulation in SC. Furthermore, higher free drug concentrations can be achieved in DM and BL when the

slow VE-release nanoparticles are used. This is mainly because of the relatively high nanoparticle concentrations in DM, as shown in **Figure 11**.

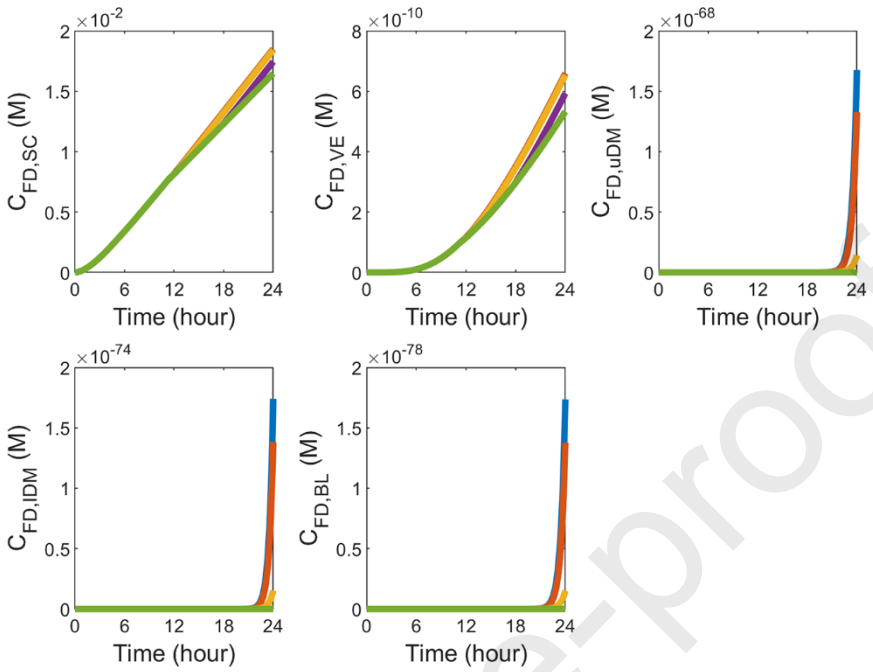

Figure 12. Time courses of free drug concentration is skin layers and blood using nanoparticles with different release rates in VE.

Figure 13 presents the delivery outcomes when using nanoparticles with different release rates in VE. Comparisons show that increasing this release rate would reduce the effectiveness in all the skin layers and blood. Furthermore, the drug exposure in DM and BL could be significantly low when $k_{\mathrm{rel,VE}} \geq 1.0 \times 10^{-3}$ s^{-1}.

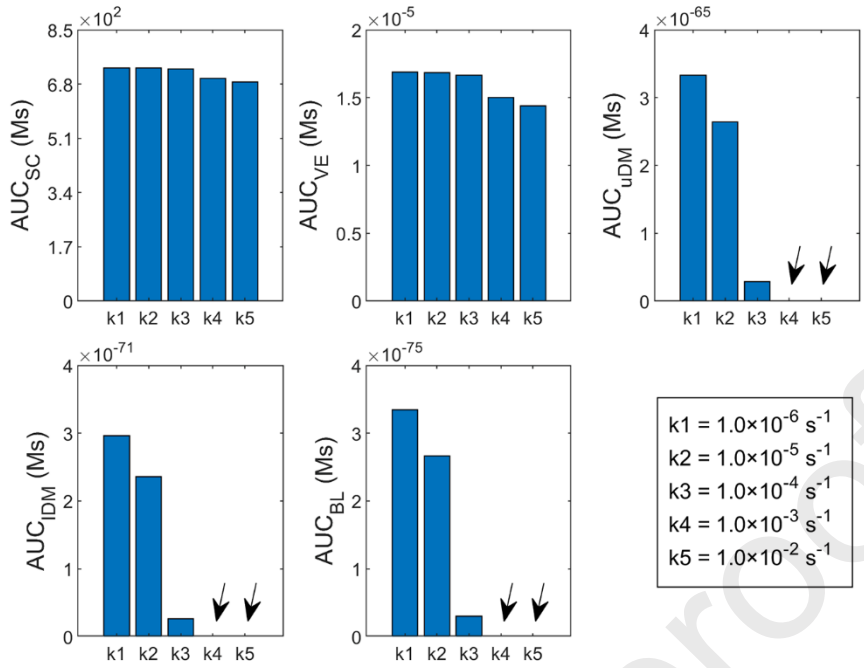

Figure 13. Drug exposure over time ($AUC_{24\text{hour}}$) of skin layers and blood using nanoparticles with different release rates in VE.

3.4. Effect of release rate in DM ($k_{\text{rel,DM}}$)

The impacts of release rate in DM on nanoparticle-encapsulated drug concentration are shown in **Figure 14**. Changing $k_{\text{rel,DM}}$ could only strongly influence the drug concentrations in DM, whereas no obvious difference can be found in the upstream layers of SC in the examined time window. Fewer drugs could be maintained in the encapsulated form in DM when the local release rate rises.

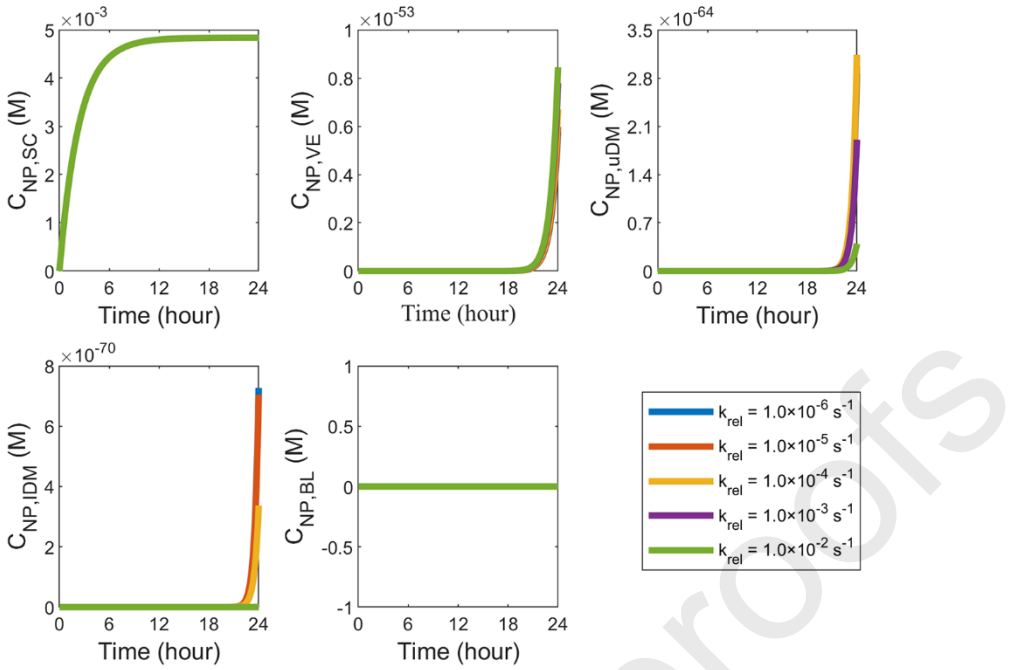

Figure 14. Time courses of nanoparticle-encapsulated drug concentration is skin layers and blood using nanoparticles with different release rates in DM.

Figure 15 shows how $k_{\mathrm{rel,DM}}$ determines the concentrations of free drugs. No obvious difference can be found in SC and VE; this is consistent with the nanoparticle-encapsulated drug concentrations shown in **Figure 14**. However, $k_{\mathrm{rel,DM}}$ affects the free drug concentration in DM in two different ways, depending on the location. Increasing $k_{\mathrm{rel,DM}}$ can effectively raise the drug concentration in uDM, as more drugs can be released locally. This is different from the results in **Figure 12**. This is because the concentration of the free drug is mainly determined by the local drug release from nanoparticles. Since both VE and DM are aqueous membranes, the transport properties of nanoparticles would not change much in these two layers, in particular the diffusivity and equivalent partition coefficient. Therefore, nanoparticles are able to continuously transport from VE to DM to provide comparable drug supplies. In contrast, the relationship between $k_{\mathrm{rel,DM}}$ and free drug concentration in lDM is non-linear. The maximum drug accumulation is obtained when the release rate reaches 1.0×10^{-4} s^{-1}. This optimal $k_{\mathrm{rel,DE}}$ is determined by the trade-off between the two sources of free drugs in lDM. On the one hand,

fewer nanoparticles could arrive in lDM when $k_{\mathrm{rel,DE}}$ is increased. This further reduces the amount of free drugs that can be released locally in lDM. On the other hand, the high concentration of free drugs in uDM enlarges the concentration gradient between uDM and lDM, enabling more free drugs transporting to lDM.

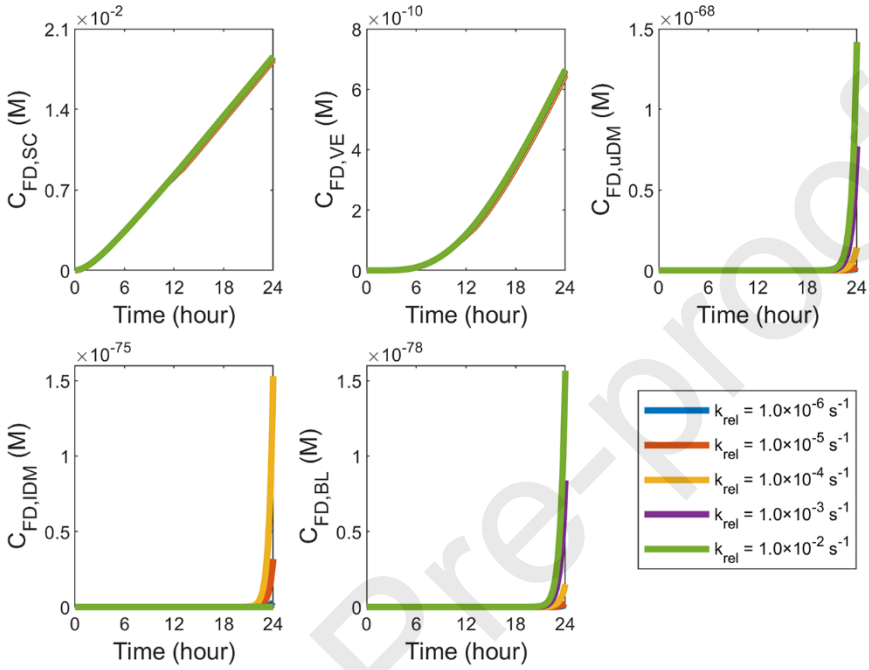

Figure 15. Time courses of free drug concentration is skin layers and blood using nanoparticles with different release rates in DM.

The treatments using nanoparticles with different DM-release rates are compared in **Figure 16**. Increasing $k_{\mathrm{rel,DM}}$ can largely improve the effectiveness in uDM. Moreover, the effectiveness of delivering drugs to lDM exhibits a non-linear correlation to this release rate, with the maximum value achieved at $k_{\mathrm{rel}} = 1.0 \times 10^{-4}$ s^{-1}. This requires $k_{\mathrm{rel,DE}}$ to be optimised to keep the trade-off between the local drug release and transport from the upstream layers, so as to maximise the treatment. The outcome of transdermal delivery of drugs into blood increase with the release rate in DM.

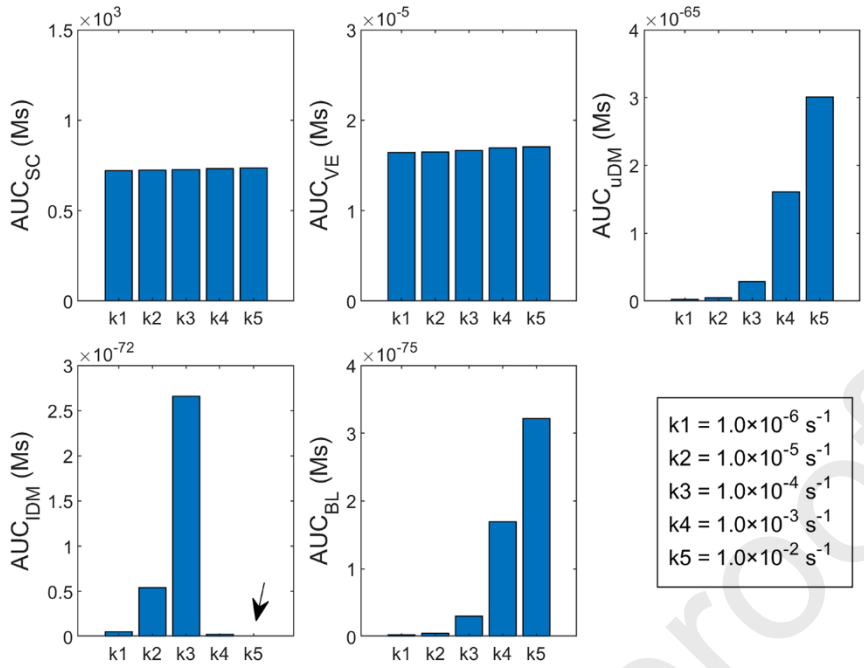

Figure 16. Drug exposure over time (AUC_{24hour}) of skin layers and blood using nanoparticles with different release rates in DM.

4. Discussion

Using nanoparticles for topical drug delivery remains under debate. The skin is commonly believed to be impermeable to nanoparticles because of the SC microstructure. On the other hand, several studies also show that this penetration is feasible [14, 15] but subject to several factors. These include the nanoparticle formulation, dimension and vehicle [16], etc. The present study is based on these findings to discuss the opportunities to improve the effectiveness of skin-penetrable nanoparticles.

Drugs need to penetrate through the skin layers of SC, VE, uDM and lDM in order in topical delivery. As a result, the characteristics of the upstream layer and local physiological and physicochemical processes (e.g. the tissue microstructure and compositions, metabolic reactions) would not only determine the delivery outcomes in the present layer but also influence the drug transport and accumulation in the downstream layers. The majority of drugs could concentrate in the top two layers of SC and VE when plain drugs are used. In contrast, although most nanoparticles still accumulate in the top two layers, nanoparticles can

successfully improve the drug penetration and accumulation in the deep sites of skin. This is due to the advantages of nanoparticles in reducing drug elimination, which is induced by the unfavourable interactions with the tissue microstructure and proteins. Consequently, the drug concentration can sustain at a relatively high level for deep penetration. Moreover, enhancing the nanoparticle SC penetration is believed to be crucial to improve the delivery outcomes. Besides the optimisation of nanoparticle formulations, several combination treatments have been developed, such as the application of ultrasound [77] and increasing the local pressure [78].

It is worth to note the concentration of drugs in VE, DM and BL remain low in the examined time window. However, a fast increase can be found at the end of this treatment cycle. This highlights the demand for a long-term drug-skin contact duration. A nanoparticle-contained hydrogel was applied once daily for seven days in the animal experiment [64]. This duration would be expected to provide an extended drug-skin contact for drugs to reach the deep sites of tissue for effective accumulation.

The outcomes of nanoparticle-mediated topical delivery remain heterogeneous, with the drug concentration decreasing throughout the skin layers from the SC surface to the deep tissue. Further increasing the drug accumulation in different depths of the skin could not only facilitate a localised treatment but also offer more flexibility in the clinical practice. As demonstrated by the modelling predictions, the remarkable sensitivities of delivery outcomes to the layer-specific release rate suggest such possibilities. Increasing the release rate in SC could improve the drug exposure in SC and VE. As shown in **Figure 10** and **Figure 13**, the release rates in SC and VE need to be controlled below a threshold for achieving effective drug exposure in DM and BL.

The drug delivery in DM can be improved by three means, including reducing the release rate in either SC or VE and increasing the release rate in DM, as shown in **Figure 10**, **Figure 13**

and **Figure 16**. Quantitative comparisons between these figures denote that the largest improvement takes place when the release rate in SC is reduced. However, this would simultaneously raise the concentration in VE. To be different, the increase of $k_{\mathrm{rel,DM}}$ has limited impacts on SC and VE, which could contribute to realising the localised drug delivery for more precise treatment.

The modelling predictions from this study demonstrate that the delivery outcomes in each skin layer are greatly sensitive to the local rate of drug release from nanoparticles. Given the heterogeneous characteristics of different skin layers, the microscale models considering the geometrical features of tissue microarchitectures are preferred to further examine the complex interactions between the nanoparticles, free drugs and tissue compositions. This is beneficial to uncover the underlying mechanisms that would in turn improve the design of topical delivery. The localised release could be realised through different means. A bespoken formulation would make the nanoparticles sensitive to the microenvironment in a specific skin layer. Moreover, the drug release dynamics can be enhanced actively using thermosensitive nanoparticles, which are designed to release the payloads only when the environmental temperature is above a threshold [79, 80]. High-intensity focused ultrasound can be used to heat the targeted lesions, and thus trigger the drug release [81, 82]. As the ultrasound projection area and penetration depth can be well controlled [83], the drug release is expected to be highly localised.

Most drugs across SC via a tortuous pathway within the lipid domain which mainly is the gaps between corneocytes. As a result, the transport of nanoparticles in SC presents a size-dependent manner. The transport is more efficient for small nanoparticles, whereas nanoparticles with a similar dimension as the lipid domain are highly possible to be completely blocked. In addition, the ability to transport in SC also depends on the nanoparticle formulation. In a diffusion chamber experiment, gold-nanoparticles were able to penetrate SC even if the dimension was greater than 100 nm [12, 84]. Lipid nanoparticles were also found to be able to pass through

the SC [18] by diffusion [85, 86]. Since there is a lack of literature reporting the nanoparticle diffusivity is SC, the value is roughly estimated as described in Section 2.3. Although this is in line with the fact that SC with the densely packed microstructure is less permeable than VE and DM that are aqueous membranes, the estimation remains less accurate. In this regard, the values of diffusivity are kept identical in all the simulations to minimise the impacts. Overall, this study can only provide qualitative results. The transport properties of specific nanoparticles, the diffusivity in particular, are needed for performing quantitative analyses. This requires further support from experiments.

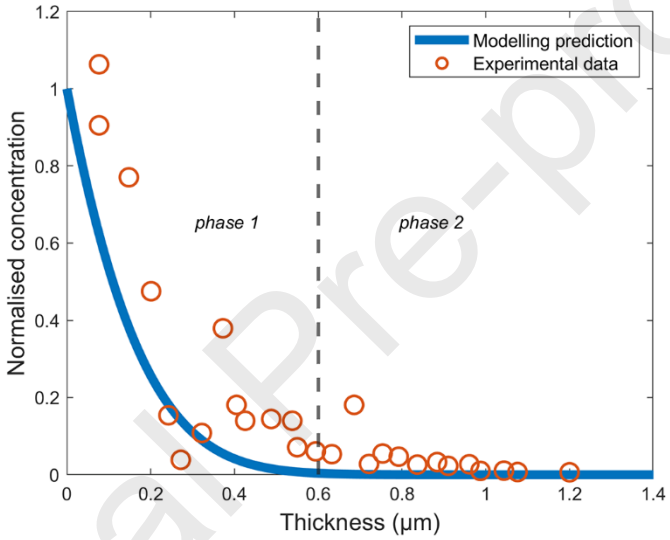

Figure 17. Comparison of experimental measurements and modelling predictions on the concentration of econazole as a function of depth in DM. Experimental data and model parameters are extracted from Ref. **[26].**

The adopted model is established to capture the key interplays between the skin tissue and drugs in the delivery processes. The modelling predicted outcome of topical delivery of econazole is compared to the experimental data [26] in **Figure 17**. The overall coefficient of determination is 0.87. The drug concentration profile is further divided into two phases with a boundary set at $x = 0.6$ μm. The coefficients of determination are 0.42 and 0.98 in phase 1 and phase 2, respectively. The predicted delivery outcomes of five more drugs are compared to experimental results in Ref. [26], with the coefficient of determination ranging from 0.33 to

0.91. The poor regression quality was attributed to the large variability of experimental data. On the one hand, the drug penetration depth is on the scale of micrometre. This consequentially raises the difficulties in accurately measuring the concentration which is location-dependent. On the other hand, the complex and heterogeneous microenvironment in skin tissue would also cause the variability of the measurement. Moreover, mathematical modelling was applied to predict the penetration of Evans blue and albumin in agarose gel, with the coefficient of determinations achieved at 0.70 and 0.83, respectively [87]. Similarly, several model validation studies using the convection-diffusion-reaction equation to predict the small molecules and nanoparticles transport have been reported in the literature [87-92]. Overall, these comparisons further highlight the importance to understand the micro-environment in tissue and to measure the transport properties of drug delivery systems. It should mention that the nanoparticles with single-phase release is used in this study. Determined by the formulation and materials, drug delivery systems could present multiple release phases [93] in order to meet the specific delivery purpose. The delivery outcomes could strongly associate with the timing of the phase change, which can be pre-designed and controlled in practice. A follow-up study could be carried out to discuss the application of nanoparticles with different release profiles in topical delivery. Moreover, the continuous non-fenestrated capillaries in skin are treated to be non-permeable to general nanoparticles due to the nanoparticle's large dimension. However, besides the nanoparticle size, the transvascular permeability of nanoparticles also depends on the formulation, particularly the ligands attached to the nanoparticle surface. For instance, transferrin can significantly improve the nanoparticle permeability to cross the blood-brain barrier [94]. This transvascular transport needs to be considered when examining the performance of specific nanoparticles with such ligands attached.

Nevertheless, a number of assumptions are involved in this study. (1) Skin layers are divided strictly with sharp boundaries as shown in **Figure 2**. The model parameters reflecting tissue

properties are homogeneous in each layer. *In vivo*, the transition zoom between two layers could be irregular. The biological properties in these zooms could be heterogeneous depending on the local microenvironment [95, 96]. These assumptions could be relaxed with supports of realistic geometry and tissue properties from microscopic images and experiments. (2) The water and drug transport through sweat glands and hair follicles is not considered. This transport process [97, 98] is determined by multiple factors including the distribution of hair follicles, depth into the skin layers and tissue microstructure around hair follicles and sweat glands, etc. This is out of the scope of this study, and the present model needs to be further developed to describe this process. (3) SC is treated as an impermeable layer to the interstitial fluid flow. This is reasonable as water mainly crosses SC in the form of vapour, driven by the gradient of water vapour pressure on both sides of the skin barrier [99]. This is usually named the trans-epidermal water loss (TEWL). As this study is focused on the drug transport in skin layers, the complex process of phase transition involved in TEWL is neglected. A mathematical model has been reported to describe this vapour escape [100]. It could be coupled with the model in this study to examine the impact of water loss on drug delivery in future. (4) The concentration of nanoparticles on the top of the skin is assumed to be constant over time [22, 25]. This assumption is introduced with the aim to focus on the drug transport inside the skin layers. Applying drug-coated cream multiple times or using drug-coated plaster and hydrogel [101] could help keep this concentration constant. Even though, this concentration could be heterogeneous in the poorly stirred vehicles [102, 103] and decreases as time proceeds [104]; these complexities depend on the type of drug formulations, nanoparticles and administration scenario including dosing and timing. A separate study can be conducted to examine the impacts of these factors in order to optimise the delivery strategy. (5) A zero-flux boundary condition is applied on the SC surface for free drugs. It is assumed that the free drugs are unable to leave the skin surface by diffusion. This would be feasible for the vehicles in which the

diffusion coefficient of free drugs is significantly low. In contrast, a non-zero flux boundary condition is needed when the free drug can effectively diffuse in the vehicle. As a result, the present model should be further developed to describe the transport process in the delivery vehicle [63]. It is worth pointing out that this SC-vehicle transport is highly dependent on the vehicle formulation and material. As this study is focused on the transport into the deep skin tissue, such a complex process is not included. A vehicle-specific study could be conducted to examine the effect of this SC-vehicle transport on the delivery outcomes. (6) Given that most capillaries are in the DM region next to VE [22, 34, 35], the function of blood drainage is only considered in this region, whereas the capillary density is assumed to be zero in lDM. This is a simplified model. It can be improved by using a distribution map of blood vessels which could be obtained by analysing patient-specific tissue microscopic images. (7) With the aim to examine the impact of release rate, the rest model parameters are assumed to be constant in this study and only representative and averaged values are used, as listed in **Table 1** and **Table 2**. *In vivo*, these model parameters would vary in wide spectrums depending on the tissue microenvironment and drug properties, such as drug diffusivity, tissue permeability and partition coefficient, etc. Separate studies should be conducted to examine their impacts [105]. More importantly, the importance of each tissue and drug property in determining the delivery outcomes could also be highly different. A follow-up study to cross-compare the role of each property will identify the most influential factors [106], and thereby provide suggestions for improving the treatment design.

5. Conclusions

Nanoparticle-mediated topical delivery is studied using mathematical modelling. Results denote that long-term drug-skin contact is essential to achieve effective drug accumulation in the deep skin tissue. As compared to the direct administration of plain drugs, nanoparticles have the potential to reduce the free drug concentrations in SC and VE, and enable more drugs

to transport into the deep skin layer of DM and BL to enhance the therapy. The delivery outcomes are highly sensitive to the drug release rate. Using nanoparticles with slow-release in SC would significantly enhance the drug accumulation in all the downstream layers. The release rates in SC and VE need to be maintained below a threshold for effective drug exposure in DM and BL. A more localised improvement in uDM can be obtained by increasing the release rate in DM. To be different, this release rate needs to be optimised to enhance the treatment in lDM. Results obtained in this study would be applied as a guide for the design and optimisation of nanoparticle-mediated topical delivery.

Declaration

The authors have declared that no competing interests exist.

References

[1] C.H. Purdon, J.M. Haigh, C. Surber, E.W. Smith, Foam drug delivery in dermatology, American Journal of Drug Delivery, 1 (2003) 71-75.

[2] M.A.C. Manoukian, C.W. Migdal, A.R. Tembhekar, J.A. Harris, C. DeMesa, Topical administration of ibuprofen for injured athletes: considerations, formulations, and comparison to oral delivery, Sports Medicine-Open, 3 (2017) 1-9.

[3] M.R. Prausnitz, R. Langer, Transdermal drug delivery, Nature Biotechnology, 26 (2008) 1261-1268.

[4] R.H. Guy, J. Hadgraft, A theoretical description relating skin penetration to the thickness of the applied medicament, International Journal of Pharmaceutics, 6 (1980) 321-332.

[5] M.R. Prausnitz, P.M. Elias, T.J. Franz, M. Schmuth, J.-C. Tsai, G.K. Menon, W.M. Holleran, K.R. Feingold, Skin barrier and transdermal drug delivery, Dermatology, 3 (2012) 2065-2073.

[6] A. Naik, Y.N. Kalia, R.H. Guy, H. Fessi, Enhancement of topical delivery from biodegradable nanoparticles, Pharmaceutical Research, 21 (2004) 1818-1825.

[7] C. Puglia, P. Blasi, L. Rizza, A. Schoubben, F. Bonina, C. Rossi, M. Ricci, Lipid nanoparticles for prolonged topical delivery: an in vitro and in vivo investigation, International Journal of Pharmaceutics, 357 (2008) 295-304.

[8] S. Küchler, M. Abdel-Mottaleb, A. Lamprecht, M.R. Radowski, R. Haag, M. Schäfer-Korting, Influence of nanocarrier type and size on skin delivery of hydrophilic agents, International Journal of Pharmaceutics, 377 (2009) 169-172.

[9] M. Ghadiri, S. Fatemi, A. Vatanara, D. Doroud, A.R. Najafabadi, M. Darabi, A.A. Rahimi, Loading hydrophilic drug in solid lipid media as nanoparticles: Statistical modeling of entrapment efficiency and particle size, International Journal of Pharmaceutics, 424 (2012) 128-137.

[10] H.I. Labouta, L.K. El-Khordagui, T. Kraus, M. Schneider, Mechanism and determinants of nanoparticle penetration through human skin, Nanoscale, 3 (2011) 4989-4999.

[11] H.I. Labouta, D.C. Liu, L.L. Lin, M.K. Butler, J.E. Grice, A.P. Raphael, T. Kraus, L.K. El-Khordagui, H.P. Soyer, M.S. Roberts, Gold nanoparticle penetration and reduced metabolism in human skin by toluene, Pharmaceutical Research, 28 (2011) 2931-2944.

[12] G. Sonavane, K. Tomoda, A. Sano, H. Ohshima, H. Terada, K. Makino, In vitro permeation of gold nanoparticles through rat skin and rat intestine: effect of particle size, Colloids and Surfaces B: Biointerfaces, 65 (2008) 1-10.

[13] M.Y. Kirillin, M.V. Shirmanova, M.A. Sirotkina, M. Bugrova, B.N. Khlebtsov, E.V. Zagainova, Contrasting properties of gold nanoshells and titanium dioxide nanoparticles for optical coherence tomography imaging of skin: Monte Carlo simulations and in vivo study, Journal of Biomedical Optics, 14 (2009) 021017.

[14] F.L. Filon, M. Mauro, G. Adami, M. Bovenzi, M. Crosera, Nanoparticles skin absorption: New aspects for a safety profile evaluation, Regulatory Toxicology and Pharmacology, 72 (2015) 310-322.

[15] T.W. Prow, J.E. Grice, L.L. Lin, R. Faye, M. Butler, W. Becker, E.M. Wurm, C. Yoong, T.A. Robertson, H.P. Soyer, Nanoparticles and microparticles for skin drug delivery, Advanced Drug Delivery Reviews, 63 (2011) 470-491.

[16] M. Roberts, Y. Mohammed, M. Pastore, S. Namjoshi, S. Yousef, A. Alinaghi, I. Haridass, E. Abd, V. Leite-Silva, H. Benson, Topical and cutaneous delivery using nanosystems, Journal of Controlled Release, 247 (2017) 86-105.

[17] A. Essaghraoui, A. Belfkira, B. Hamdaoui, C. Nunes, S.A.C. Lima, S. Reis, Improved dermal delivery of cyclosporine a loaded in solid lipid nanoparticles, Nanomaterials, 9 (2019) 1204.

[18] T. Moniz, S.A.C. Lima, S. Reis, Application of the human stratum corneum lipid-based mimetic model in assessment of drug-loaded nanoparticles for skin administration, International Journal of Pharmaceutics, 591 (2020) 119960.

[19] W. Zhan, M. Alamer, X.Y. Xu, Computational modelling of drug delivery to solid tumour: Understanding the interplay between chemotherapeutics and biological system for optimised delivery system, Advanced Drug Delivery Reviews, 132 (2018) 81-103.

[20] C. Liu, J. Krishnan, J. Stebbing, X.Y. Xu, Use of mathematical models to understand anticancer drug delivery and its effect on solid tumors, Pharmacogenomics, 12 (2011) 1337-1348.

[21] C.M. Groh, M.E. Hubbard, P.F. Jones, P.M. Loadman, N. Periasamy, B.D. Sleeman, S.W. Smye, C.J. Twelves, R.M. Phillips, Mathematical and computational models of drug transport in tumours, Journal of The Royal Society Interface, 11 (2014) 20131173.

[22] Y.G. Anissimov, O.G. Jepps, Y. Dancik, M.S. Roberts, Mathematical and pharmacokinetic modelling of epidermal and dermal transport processes, Advanced Drug Delivery Reviews, 65 (2013) 169-190.

[23] M.S. Roberts, S. Cross, Y. Anissimov, Factors affecting the formation of a skin reservoir for topically applied solutes, Skin Pharmacology and Physiology, 17 (2004) 3-16.

[24] R.H. Guy, J. Hadgraft, Physicochemical interpretation of the pharmacokinetics of percutaneous absorption, Journal of Pharmacokinetics and BBiopharmaceutics, 11 (1983) 189-203.

[25] N. Seko, H. Bando, C.W. Lim, F. Yamashita, M. Hashida, Theoretical analysis of the effect of cutaneous metabolism on skin permeation of parabens based on a two-layer skin diffusion/metabolism model, Biological and Pharmaceutical Bulletin, 22 (1999) 281-287.

[26] Y.G. Anissimov, M.S. Roberts, Modelling dermal drug distribution after topical application in human, Pharmaceutical Research, 28 (2011) 2119-2129.

[27] M.E. Lane, Skin penetration enhancers, International journal of pharmaceutics, 447 (2013) 12-21.

[28] K. Kretsos, G.B. Kasting, A geometrical model of dermal capillary clearance, Mathematical Biosciences, 208 (2007) 430-453.

[29] J.J. Calcutt, Y.G. Anissimov, Predicting viable skin concentration: Diffusional and convective drug transport, Journal of Pharmaceutical Sciences, 110 (2021) 2823-2832.

[30] D. Feuchter, M. Heisig, G. Wittum, A geometry model for the simulation of drug diffusion through the stratum corneum, Computing and Visualization in Science, 9 (2006) 117-130.

[31] B.R. Masters, P.T. So, Confocal microscopy and multi-photon excitation microscopy of human skin in vivo, Optics Express, 8 (2001) 2-10.

[32] E. Touitou, Drug delivery across the skin, Expert opinion on biological therapy, 2 (2002) 723-733.

[33] X. Li, U. Dinish, J. Aguirre, R. Bi, K. Dev, A.B.E. Attia, S. Nitkunanantharajah, Q.H. Lim, M. Schwarz, Y.W. Yew, Optoacoustic mesoscopy analysis and quantitative estimation of specific imaging metrics in Fitzpatrick skin phototypes II to V, Journal of Biophotonics, 12 (2019) e201800442.

[34] I.M. Braverman, The cutaneous microcirculation, in: Journal of Investigative Dermatology Symposium Proceedings, Elsevier, 2000, pp. 3-9.

[35] I.M. Braverman, A. Keh, D. Goldminz, Correlation of laser Doppler wave patterns with underlying microvascular anatomy, Journal of Investigative Dermatology, 95 (1990) 283-286.

[36] M. Skobe, M. Detmar, Structure, function, and molecular control of the skin lymphatic system, in: Journal of Investigative Dermatology Symposium Proceedings, Elsevier, 2000, pp. 14-19.

[37] L.T. Baxter, R.K. Jain, Transport of fluid and macromolecules in tumors. I. Role of interstitial pressure and convection, Microvascular Research, 37 (1989) 77-104.

[38] Y.G. Anissimov, M.S. Roberts, Diffusion modelling of percutaneous absorption kinetics: 4. Effects of a slow equilibration process within stratum corneum on absorption and desorption kinetics, Journal of Pharmaceutical Sciences, 98 (2009) 772-781.

[39] W. Zhan, C.-H. Wang, Convection enhanced delivery of liposome encapsulated doxorubicin for brain tumour therapy, Journal of Controlled Release, 285 (2018) 212-229.

[40] Y.-M.F. Goh, H.L. Kong, C.-H. Wang, Simulation of the delivery of doxorubicin to hepatoma, Pharmaceutical Research, 18 (2001) 761-770.

[41] R. Molinaro, J.O. Martinez, A. Zinger, A. De Vita, G. Storci, N. Arrighetti, E. De Rosa, K.A. Hartman, N. Basu, N. Taghipour, Leukocyte-mimicking nanovesicles for effective doxorubicin delivery to treat breast cancer and melanoma, Biomaterials Science, 8 (2020) 333-341.

[42] E. Berman, E. Casper, J. Howard, R. Wittes, Phase II trial of 4'-epi-doxorubicin in patients with advanced malignant melanoma, Cancer Treatment Reports, 68 (1984) 679-680.

[43] D.A. Vorobiof, B.L. Rapoport, R. Mahomed, M. Karime, Phase II study of pegylated liposomal doxorubicin in patients with metastatic malignant melanoma failing standard chemotherapy treatment, Melanoma Research, 13 (2003) 201-203.

[44] G. Champsas, O. Papadopoulos, The Role of the Sentinel Lymph Node Biopsy in the Treatment of Nonmelanoma Skin Cancer and Cutaneous Melanoma, in: Non-Melanoma Skin Cancer and Cutaneous Melanoma, Springer, 2020, pp. 647-704.

[45] Q.D. Chu, J.F. Gibbs, G.B. Zibari, Surgical oncology: a practical and comprehensive approach, Springer, 2014.

[46] Y. Lee, K. Hwang, Skin thickness of Korean adults, Surgical and Radiologic Anatomy, 24 (2002) 183-189.

[47] D.Y. Arifin, K.Y.T. Lee, C.-H. Wang, Chemotherapeutic drug transport to brain tumor, Journal of Controlled Release, 137 (2009) 203-210.

[48] M. Roberts, W. Pugh, J. Hadgraft, Epidermal permeability: penetrant structure relationships. 2. The effect of H-bonding groups in penetrants on their diffusion through the stratum corneum, International Journal of Pharmaceutics, 132 (1996) 23-32.

[49] S.W. Chung, G.C. Kim, S. Kweon, H. Lee, J.U. Choi, F. Mahmud, H.W. Chang, J.W. Kim, W.-C. Son, S.Y. Kim, Metronomic oral doxorubicin in combination of Chk1 inhibitor MK-8776 for p53-deficient breast cancer treatment, Biomaterials, 182 (2018) 35-43.

[50] X. Zhang, X. Sun, J. Li, X. Zhang, T. Gong, Z. Zhang, Lipid nanoemulsions loaded with doxorubicin-oleic acid ionic complex: characterization, in vitro and in vivo studies, Die Pharmazie-An International Journal of Pharmaceutical Sciences, 66 (2011) 496-505.

[51] F. Yurt, M. Ince, S.G. Colak, K. Ocakoglu, O. Er, H.M. Soylu, C. Gunduz, C.B. Avci, C.C. Kurt, Investigation of in vitro PDT activities of zinc phthalocyanine immobilised TiO2 nanoparticles, International Journal of Pharmaceutics, 524 (2017) 467-474.

[52] Q.-Y. Bao, A.-Y. Liu, Y. Ma, H. Chen, J. Hong, W.-B. Shen, C. Zhang, Y. Ding, The effect of oil-water partition coefficient on the distribution and cellular uptake of liposome-encapsulated gold nanoparticles, Colloids and Surfaces B: Biointerfaces, 146 (2016) 475-481.

[53] K. Kretsos, M.A. Miller, G. Zamora-Estrada, G.B. Kasting, Partitioning, diffusivity and clearance of skin permeants in mammalian dermis, International Journal of Pharmaceutics, 346 (2008) 64-79.

[54] R. Tong, H.D. Hemmati, R. Langer, D.S. Kohane, Photoswitchable nanoparticles for triggered tissue penetration and drug delivery, Journal of the American Chemical Society, 134 (2012) 8848-8855.

[55] C. Wong, T. Stylianopoulos, J. Cui, J. Martin, V.P. Chauhan, W. Jiang, Z. Popović, R.K. Jain, M.G. Bawendi, D. Fukumura, Multistage nanoparticle delivery system for deep penetration into tumor tissue, Proceedings of the National Academy of Sciences, 108 (2011) 2426-2431.

[56] A. Zhang, X. Mi, L.X. Xu, Study of Thermally Targeted Nano-Particle Drug Delivery for Tumor Therapy, in: International Conference on Micro/Nanoscale Heat Transfer, 2008, pp. 1399-1406.

[57] B.M. Magnusson, Y.G. Anissimov, S.E. Cross, M.S. Roberts, Molecular size as the main determinant of solute maximum flux across the skin, Journal of Investigative Dermatology, 122 (2004) 993-999.

[58] T. Tagami, M.J. Ernsting, S.-D. Li, Optimization of a novel and improved thermosensitive liposome formulated with DPPC and a Brij surfactant using a robust in vitro system, Journal of Controlled Release, 154 (2011) 290-297.

[59] J. Connor, M.B. Yatvin, L. Huang, pH-sensitive liposomes: acid-induced liposome fusion, Proceedings of the National Academy of Sciences, 81 (1984) 1715-1718.

[60] T. Tagami, J.P. May, M.J. Ernsting, S.-D. Li, A thermosensitive liposome prepared with a Cu 2+ gradient demonstrates improved pharmacokinetics, drug delivery and antitumor efficacy, Journal of Controlled Release, 161 (2012) 142-149.

[61] E. Garcion, A. Lamprecht, B. Heurtault, A. Paillard, A. Aubert-Pouessel, B. Denizot, P. Menei, J.-P. Benoît, A new generation of anticancer, drug-loaded, colloidal vectors reverses multidrug resistance in glioma and reduces tumor progression in rats, Molecular Cancer Therapeutics, 5 (2006) 1710-1722.

[62] A. Hussain, A. Samad, S. Singh, M. Ahsan, M. Haque, A. Faruk, F. Ahmed, Nanoemulsion gel-based topical delivery of an antifungal drug: in vitro activity and in vivo evaluation, Drug Delivery, 23 (2016) 642-657.

[63] M. Abrami, S. Golob, F. Pontelli, G. Chiarappa, G. Grassi, B. Perissutti, D. Voinovich, N. Halib, L. Murena, G. Milcovich, Antibacterial drug release from a biphasic gel system: Mathematical modelling, International Journal of Pharmaceutics, 559 (2019) 373-381.

[64] W. Gao, D. Vecchio, J. Li, J. Zhu, Q. Zhang, V. Fu, J. Li, S. Thamphiwatana, D. Lu, L. Zhang, Hydrogel containing nanoparticle-stabilized liposomes for topical antimicrobial delivery, Acs Nano, 8 (2014) 2900-2907.

[65] R.L. Cleek, A.L. Bunge, A new method for estimating dermal absorption from chemical exposure. 1. General approach, Pharmaceutical Research, 10 (1993) 497-506.

[66] C.S. Teo, W.H.K. Tan, T. Lee, C.-H. Wang, Transient interstitial fluid flow in brain tumors: Effect on drug delivery, Chemical Engineering Science, 60 (2005) 4803-4821.

[67] E. Renkin, C. Michel, Capillary permeability to small solutes, Handbook of Physiology: The Cardiovascular system, Microcirculation, (1984).

[68] K. Kretsos, G. Kasting, Dermal capillary clearance: physiology and modeling, Skin pharmacology and physiology, 18 (2005) 55-74.

[69] H. Xu, M. Hu, X. Yu, Y. Li, Y. Fu, X. Zhou, D. Zhang, J. Li, Design and evaluation of pH-sensitive liposomes constructed by poly (2-ethyl-2-oxazoline)-cholesterol hemisuccinate for doxorubicin delivery, European Journal of Pharmaceutics and Biopharmaceutics, 91 (2015) 66-74.

[70] P. Boderke, K. Schittkowski, M. Wolf, H.P. Merkle, Modeling of diffusion and concurrent metabolism in cutaneous tissue, Journal of Theoretical Biology, 204 (2000) 393-407.

[71] S. Eikenberry, A tumor cord model for doxorubicin delivery and dose optimization in solid tumors, Theoretical Biology and Medical Modelling, 6 (2009) 16-35.

[72] W. Zhan, F. Rodriguez y Baena, D. Dini, Effect of tissue permeability and drug diffusion anisotropy on convection-enhanced delivery, Drug delivery, 26 (2019) 773-781.

[73] M. Takada, S. Hattori, Presence of fenestrated capillaries in the skin, The Anatomical Record, 173 (1972) 213-219.

[74] J. Gao, Z. Wang, H. Liu, L. Wang, G. Huang, Liposome encapsulated of temozolomide for the treatment of glioma tumor: preparation, characterization and evaluation, Drug Discoveries & Therapeutics, 9 (2015) 205-212.

[75] A. Gabizon, R. Catane, B. Uziely, B. Kaufman, T. Safra, R. Cohen, F. Martin, A. Huang, Y. Barenholz, Prolonged circulation time and enhanced accumulation in malignant exudates of doxorubicin encapsulated in polyethylene-glycol coated liposomes, Cancer Research, 54 (1994) 987-992.

[76] R.S. Kadam, D.W. Bourne, U.B. Kompella, Nano-advantage in enhanced drug delivery with biodegradable nanoparticles: contribution of reduced clearance, Drug Metabolism and Disposition, 40 (2012) 1380-1388.

[77] N. Zhang, Y. Wu, R. Xing, B. Xu, D. Guoliang, P. Wang, Effect of ultrasound-enhanced transdermal drug delivery efficiency of nanoparticles and brucine, BioMed Research International, 2017 (2017).

[78] D.C.S. Lio, R.N. Chia, M.S.Y. Kwek, C. Wiraja, L.E. Madden, H. Chang, S.M.A. Khadir, X. Wang, D.L. Becker, C. Xu, Temporal pressure enhanced topical drug delivery through micropore formation, Science Advances, 6 (2020) eaaz6919.

[79] X. Zhang, P.F. Luckham, A.D. Hughes, S. Thom, X.Y. Xu, Towards an understanding of the release behavior of temperature-sensitive liposomes: a possible explanation of the "pseudoequilibrium" release behavior at the phase transition temperature, Journal of Liposome Research, 23 (2013) 167-173.

[80] R.M. Staruch, M. Ganguly, I.F. Tannock, K. Hynynen, R. Chopra, Enhanced drug delivery in rabbit VX2 tumours using thermosensitive liposomes and MRI-controlled focused ultrasound hyperthermia, International Journal of Hyperthermia, 28 (2012) 776-787.

[81] M.D. Gray, P.C. Lyon, C. Mannaris, L.K. Folkes, M. Stratford, L. Campo, D.Y. Chung, S. Scott, M. Anderson, R. Goldin, Focused ultrasound hyperthermia for targeted drug release from thermosensitive liposomes: results from a phase I trial, Radiology, 291 (2019) 232-238.

[82] W. Zhan, W. Gedroyc, X.Y. Xu, Towards a multiphysics modelling framework for thermosensitive liposomal drug delivery to solid tumour combined with focused ultrasound hyperthermia, Biophysics Reports, 5 (2019) 43-59.

[83] P.C. Lyon, C. Mannaris, M. Gray, R. Carlisle, F.V. Gleeson, D. Cranston, F. Wu, C.C. Coussios, Large-volume hyperthermia for safe and cost-effective targeted drug delivery using a clinical ultrasound-guided focused ultrasound device, Ultrasound in Medicine & Biology, 47 (2021) 982-997.

[84] G. Raju, N. Katiyar, S. Vadukumpully, S.A. Shankarappa, Penetration of gold nanoparticles across the stratum corneum layer of thick-Skin, Journal of Dermatological Science, 89 (2018) 146-154.

[85] N. Weiner, N. Williams, G. Birch, C. Ramachandran, C. Shipman Jr, G. Flynn, Topical delivery of liposomally encapsulated interferon evaluated in a cutaneous herpes guinea pig model, Antimicrobial Agents and Chemotherapy, 33 (1989) 1217-1221.

[86] J. Brewer, M. Bloksgaard, J. Kubiak, J.A. Sørensen, L.A. Bagatolli, Spatially resolved two-color diffusion measurements in human skin applied to transdermal liposome penetration, Journal of Investigative Dermatology, 133 (2013) 1260-1268.

[87] K. Neeves, C. Lo, C. Foley, W. Saltzman, W. Olbricht, Fabrication and characterization of microfluidic probes for convection enhanced drug delivery, Journal of Controlled Release, 111 (2006) 252-262.

[88] A.A. Linninger, M.R. Somayaji, M. Mekarski, L. Zhang, Prediction of convection-enhanced drug delivery to the human brain, Journal of Theoretical Biology, 250 (2008) 125-138.

[89] A.A. Linninger, M.R. Somayaji, L. Zhang, M.S. Hariharan, R.D. Penn, Rigorous mathematical modeling techniques for optimal delivery of macromolecules to the brain, IEEE Transactions on Biomedical Engineering, 55 (2008) 2303-2313.

[90] W. Zhan, D.Y. Arifin, T.K. Lee, C.-H. Wang, Mathematical Modelling of Convection Enhanced Delivery of Carmustine and Paclitaxel for Brain Tumour Therapy, Pharmaceutical Research, 34 (2017) 860-873.

[91] S.H. Ranganath, Y. Fu, D.Y. Arifin, I. Kee, L. Zheng, H.-S. Lee, P.K.-H. Chow, C.-H. Wang, The use of submicron/nanoscale PLGA implants to deliver paclitaxel with enhanced pharmacokinetics and therapeutic efficacy in intracranial glioblastoma in mice, Biomaterials, 31 (2010) 5199-5207.

[92] W. Zhan, Convection enhanced delivery of anti-angiogenic and cytotoxic agents in combination therapy against brain tumour, European Journal of Pharmaceutical Sciences, 141 (2020) 105094.

[93] D.Y. Arifin, L.Y. Lee, C.-H. Wang, Mathematical modeling and simulation of drug release from microspheres: Implications to drug delivery systems, Advanced Drug Delivery Reviews, 58 (2006) 1274-1325.

[94] C. Lei, P. Davoodi, W. Zhan, P.K.-H. Chow, C.-H. Wang, Development of nanoparticles for drug delivery to brain tumor: the effect of surface materials on penetration into brain tissue, Journal of Pharmaceutical Sciences, 108 (2019) 1736-1745.

[95] B. Mueller, Y.G. Anissimov, M.S. Roberts, Unexpected clobetasol propionate profile in human stratum corneum after topical application in vitro, Pharmaceutical Research, 20 (2003) 1835-1837.

[96] P.A. Kolarsick, M.A. Kolarsick, C. Goodwin, Anatomy and physiology of the skin, Journal of the Dermatology Nurses' Association, 3 (2011) 203-213.

[97] A. Patzelt, J. Lademann, Drug delivery to hair follicles, Expert Opinion on Drug Delivery, 10 (2013) 787-797.

[98] J. Lademann, H. Richter, A. Teichmann, N. Otberg, U. Blume-Peytavi, J. Luengo, B. Weiss, U.F. Schaefer, C.-M. Lehr, R. Wepf, Nanoparticles–an efficient carrier for drug delivery into the hair follicles, European Journal of Pharmaceutics and Biopharmaceutics, 66 (2007) 159-164.

[99] V. Rogiers, EEMCO guidance for the assessment of transepidermal water loss in cosmetic sciences, Skin Pharmacology and Physiology, 14 (2001) 117-128.

[100] X. Li, R. Johnson, B. Weinstein, E. Wilder, E. Smith, G.B. Kasting, Dynamics of water transport and swelling in human stratum corneum, Chemical Engineering Science, 138 (2015) 164-172.

[101] K.-L. Mao, Z.-L. Fan, J.-D. Yuan, P.-P. Chen, J.-J. Yang, J. Xu, D.-L. ZhuGe, B.-H. Jin, Q.-Y. Zhu, B.-X. Shen, Skin-penetrating polymeric nanoparticles incorporated in silk fibroin hydrogel for topical delivery of curcumin to improve its therapeutic effect on psoriasis mouse model, Colloids and Surfaces B: Biointerfaces, 160 (2017) 704-714.

[102] K. Kakemi, H. Kameda, M. Kakemi, M. Ueda, T. Koizumi, Model studies on percutaneous absorption and transport in the ointment. I. Theoretical aspects, Chemical and Pharmaceutical Bulletin, 23 (1975) 2109-2113.

[103] M.S. Roberts, Y.G. Anissimov, Mathematical models in percutaneous absorption, CRC Press, 2005.

[104] Y.G. Anissimov, M.S. Roberts, Diffusion modeling of percutaneous absorption kinetics: 2. Finite vehicle volume and solvent deposited solids, Journal of Pharmaceutical Sciences, 90 (2001) 504-520.

[105] W. Zhan, Delivery of liposome encapsulated temozolomide to brain tumour: Understanding the drug transport for optimisation, International Journal of Pharmaceutics, 557 (2019) 280-292.

[106] C. Liu, X.Y. Xu, A systematic study of temperature sensitive liposomal delivery of doxorubicin using a mathematical model, Computers in Biology and Medicine, 60 (2015) 107-116.

Graphical abstract

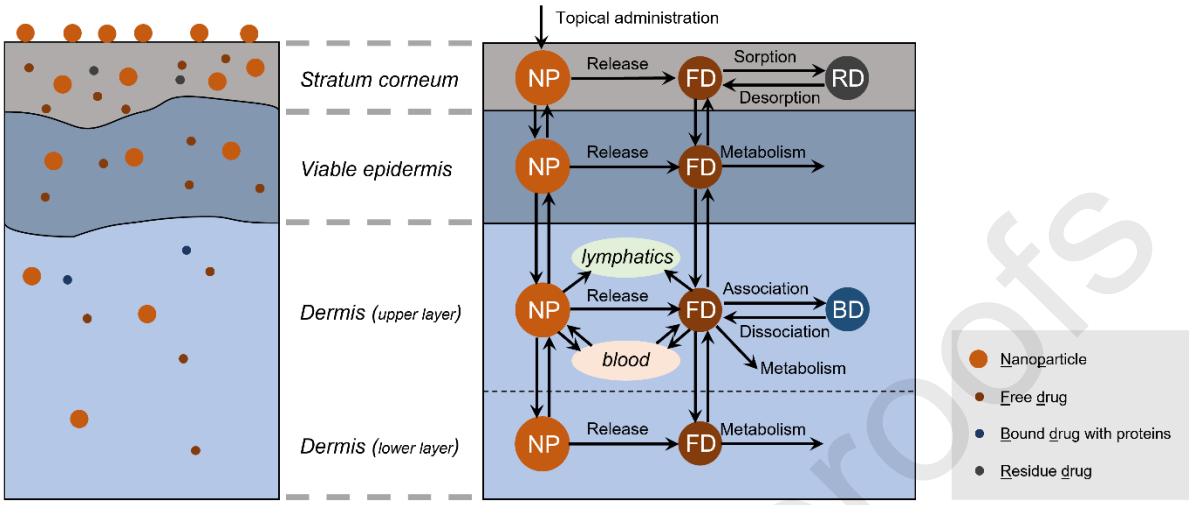

Highlights

- Nanoparticle has the potential to improve the drug accumulation in deep skin tissue.
- Drug penetration in different skin layers is sensitive to the release rate.
- Controlling the release rate can increase the drug concentration in specific layers.

Credit Author Statement

Kevin Mclean: Methodology, Visualisation, Formal analysis, Writing – Original draft preparation

Wenbo Zhan: Conceptualisation, Software, Writing – Reviewing and Editing

Declaration of interests

☒ The authors declare that they have no known competing financial interests or personal relationships that could have appeared to influence the work reported in this paper.

☐The authors declare the following financial interests/personal relationships which may be considered as potential competing interests: